

# High order discretely well-balanced finite volume methods for Euler equations with gravity - without any à priori information about the hydrostatic solution

Jonas P. Berberich · Roger Käppeli · Praveen Chandrashekar · Christian Klingenberg

Received: date / Accepted: date

**Abstract** We introduce novel high order well-balanced finite volume methods for the full compressible Euler system with gravity source term. They require no à priori knowledge of the hydrostatic solution which is to be well-balanced and are not restricted to certain classes of hydrostatic solutions. In one spatial dimension and under the assumption of an ideal gas law we construct a method that exactly balances a high order discretization of any hydrostatic state. The method is extended to general equations of state and two spatial dimensions using a local high order approximation of any hydrostatic state in each cell. The proposed methods are simple, flexible, and robust. Numerical tests verify that the well-balanced method improves the capability to accurately resolve small perturbations on hydrostatic states.

**Keywords** finite-volume methods · well-balancing · hyperbolic balance laws · compressible Euler equations with gravity · hydrostatic equilibrium · high order methods

**Mathematics Subject Classification (2010)** MSC 74S10 · 76N15 · 76M12 · 85A30

**Acknowledgements** Roger Käppeli acknowledges support by the Swiss National Science Foundation (SNSF) under grant 200021-169631. Praveen Chandrashekar would like to acknowledge support from the Department of Atomic Energy, Government of India, under project no. 12-R&D-TFR-5.01-0520.

---

J. P. Berberich (corresponding author), C. Klingenberg  
Dept. of Mathematics, Univ. of Würzburg, Emil-Fischer-Straße 40, 97074 Würzburg, Germany  
E-mail: jonas.berberich@mathematik.uni-wuerzburg.de, klingen@mathematik.uni-wuerzburg.de  
ORCID ID: 0000-0003-2598-1792 (J. P. Berberich), 0000-0003-2033-8204 (C. Klingenberg)

R. Käppeli  
Seminar for Applied Mathematics (SAM), Department of Mathematics, ETH Zürich, CH-8092 Zürich, Switzerland  
E-mail: roger.kaeppli@sam.math.ethz.ch

P. Chandrashekar  
TIFR Center for Applicable Mathematics, Bengaluru, Karnataka 560065, India  
E-mail: praveen@tifrbng.res.in  
ORCID ID: 0000-0003-1903-4107

## 1 Introduction

Compressible Euler equations arise as a model for flow of inviscid compressible fluids such as air in many applications. Finite volume methods are commonly utilized to numerically approximate solutions of this system since they are conservative and capable of resolving shocks by construction. Fluid dynamics in atmospheres can be modeled by adding a gravity source term to the Euler system. This gives rise to a new class of non-trivial static solutions, the *hydrostatic solutions*. They are described by the *hydrostatic equation*

$$\nabla p = -\rho \mathbf{g} \quad (1)$$

which models the balance between the gravity  $-\rho \mathbf{g}$ , where  $\rho$  is the gas *density* and  $\mathbf{g}$  is the *gravitational acceleration*, and the pressure gradient  $\nabla p$ , where  $p$  is the gas *pressure*. Additionally, the solution must satisfy the constitutive relation between pressure, density, and *internal energy density*  $\varepsilon$ . This relation is called *equation of state* (EoS) and it has to be added to the Euler system to close it. The EoS accounts for fluid properties such as e.g. molecular structure and internal attractive or repulsive forces. In many simulations dynamics are considered which are close to a hydrostatic state. Standard finite volume methods usually introduce truncation errors to hydrostatic states, which can be larger than the actual perturbations related to the simulated dynamical process. Hence, the small-scale dynamics can only be resolved on very fine grids, which leads to high computational cost. This creates the demand for so-called *well-balanced* methods which are constructed to be free of a truncation error at hydrostatic states.

The idea of well-balanced methods is very common especially for the shallow water equations with bottom topography. The hydrostatic solution for the shallow water equations, the so called lake-at-rest solution, can be given in the form of an algebraic relation. The lake-at-rest solutions for a certain bottom topography are unique up to an additional constant. This favors the construction of well-balanced methods since the algebraic relation can be used to perform a local hydrostatic reconstruction, which is the main tool to construct well-balanced methods. Examples can be found in [7, 36, 1, 43, 44, 58, 11] and references therein. Also, for the Ripa model, which is closely related to shallow water, there are well-balanced methods (e.g. [52, 21] and references therein).

For the compressible Euler equations with gravity source term the situation is more complicated, since the hydrostatic states are not given by an algebraic relation but by a differential equation (Eq. (1)) together with an EoS. Especially complicated EoS can increase the difficulty of performing a local hydrostatic reconstruction. The result is that there do not exist methods which are well-balanced for all EoS and all types of hydrostatic solutions, and all existing methods so far known for Euler equations with gravity bear some restriction. In one approach, methods are developed to well-balance certain classes of hydrostatic solutions. Other hydrostatic states still lead to truncation errors. Examples are given in [9, 35, 38, 19, 29, 15, 20, 22, 53, 16] and there are also higher order methods [57, 23]. The restriction to certain classes of hydrostatic solutions usually also manifests in a restriction to the EoS, which is in most cases the ideal gas EoS.

A second approach assumes à priori knowledge of the hydrostatic state which is to be well-balanced. This allows the methods to be more general, such that they can balance arbitrary hydrostatic states to arbitrary EoS (e.g. [3, 49, 5, 28]). High order methods of this type are given in [10] for one spatial dimension and in [31] for two spatial dimensions. The most general well-balanced method of this type is presented in [4]. It can be applied to balance any stationary solution and follow any time-dependent solution exactly in a high order method. It can be utilized for any multi-dimensional hyperbolic balance law. In many applications the hydrostatic solution which is of interest is known à priori, either analytically or as discrete data.

However, there are also situations, in which this is not the case. If the relevant hydrostatic state is not known and can not be expected to be of one of the classes balanced in the first type of methods (for example because a complicated non-ideal gas EoS is used), a method following the third approach can be useful. These methods are based on balancing some approximation to any hydrostatic state.

The second order methods introduced in [30, 56], for example, are exactly well-balanced for certain classes of hydrostatic states; otherwise they balance a second order discretization to any hydrostatic state. To our knowledge, there is not yet a high order method of this type in literature.

Note that this classification into three different approaches is not strict. Many methods of the third type, for example, can also be seen to be from the first type, since they also might balance certain classes of solutions exactly (e.g. [29, 56]).

In the present article, we develop a method following the third approach. A high order accurate discrete approximation to a hydrostatic state is constructed based on the density and gravitational acceleration. Well-balancing is then, following e.g. [23, 4], achieved using hydrostatic reconstruction in the manner of [1] and a suitable source term discretization. For one spatial dimension and an ideal gas EoS, it can be shown that a global high order discretization of any hydrostatic state can be well-balanced exactly. The method is extended to general EoS and two spatial dimensions using a local approximation to the hydrostatic state in each cell. Numerical tests validate a significant increase of accuracy on small perturbations to hydrostatic states. An increased order of accuracy in the convergence to exact hydrostatic states is observed in one and two spatial dimensions.

The rest of the article is structured as follows: In Section 2.1 the one-dimensional compressible Euler equations with gravity source term are introduced. A standard high order finite volume method for these is revised in Section 2.2. In Section 2.3 we develop the discretely well-balanced method (DWB) which can be applied for ideal gas. The well-balanced property and high order accuracy are stated in Theorem 2.1. The method is modified in Section 2.4 to reduce the stencil and the local approximation method (LA) is obtained. An algorithm for arbitrary EoS is added in Section 2.4.3. In Section 3, numerical experiments in one spatial dimension are conducted. It is verified numerically that the DWB method is exactly well-balanced on the discrete approximation to a hydrostatic state and DWB and LA methods are numerically shown to converge towards exact hydrostatic states with an increased order of convergence (Section 3.1). The capability of the methods to accurately resolve small perturbations on hydrostatic states is illustrated in Section 3.2. Tests with a non-ideal gas EoS are presented in Section 3.3. In Section 3.4 we verify the robustness of the methods in the presence of discontinuities. Section 4 is dedicated to the extension to two spatial dimensions. In Section 4.1 we introduce the two-dimensional Euler equations with gravity source term. Subsequently, the LA method is extended to two spatial dimensions (Section 4.3). In Section 5, numerical tests of the LA method in two spatial dimensions are presented. On a two-dimensional polytrope, which is a hydrostatic state, the increased order of accuracy is observed also for two spatial dimensions (Section 5.1). A perturbation is added to the polytrope in Section 5.2. Rayleigh–Taylor instabilities on a radial setup are simulated in Section 5.3 and the increased accuracy of the LA method is shown. In Section 6 we close the article with some conclusions and an outlook.

## 2 One-dimensional finite volume methods

### 2.1 One-dimensional compressible Euler equations with gravity

We consider the one-dimensional compressible Euler equations with gravitation in Cartesian coordinates and write them in the following compact form

$$\partial_t \mathbf{q} + \partial_x \mathbf{f} = \mathbf{s}, \quad (2)$$

where

$$\mathbf{q} = \begin{pmatrix} \rho \\ \rho u \\ E \end{pmatrix}, \quad \mathbf{f}(\mathbf{q}) = \begin{pmatrix} \rho u \\ \rho u^2 + p \\ u(E + p) \end{pmatrix} \quad \text{and} \quad \mathbf{s}(\mathbf{q}, g) = - \begin{pmatrix} 0 \\ \rho g \\ \rho u g \end{pmatrix} \quad (3)$$

are the vectors of conserved variables, fluxes and source terms, respectively. Moreover, we denote the primitive variables by  $\mathbf{w} = [\rho, u, p]^T$ . The equation of state (EoS) closes the system by relating the pressure  $p$  to the density  $\rho$  and internal energy density  $\varepsilon$ , i.e.  $p = p_{\text{EoS}}(\rho, \varepsilon)$ . A simple EoS is provided by the ideal gas law

$$p = (\gamma - 1)\varepsilon, \quad (4)$$

where  $\gamma$  is the ratio of specific heats. However, we stress that the well-balanced schemes elaborated below are not restricted to any particular EoS, which is important especially in astrophysical applications.

Next, we shortly outline a standard high-order finite volume scheme in order to fix the notation and set the stage for the detailed presentation of our novel well-balanced schemes.

## 2.2 Standard high-order finite volume methods

The spatial domain of interest  $\Omega$  is discretized into a finite number  $N$  of cells or finite volumes  $\Omega_i = [x_{i-\frac{1}{2}}, x_{i+\frac{1}{2}}]$ ,  $i = 1, \dots, N$ . The  $x_{i\mp\frac{1}{2}}$  denote the left/right cell interfaces and the point  $x_i = (x_{i-\frac{1}{2}} + x_{i+\frac{1}{2}})/2$  is the cell center.

A semi-discrete finite volume scheme is then obtained by integrating Eq. (2) over a cell  $\Omega_i$

$$\partial_t \hat{\mathbf{Q}}_i(t) = \mathcal{L}(\hat{\mathbf{Q}}_i) = -\frac{1}{\Delta x} [\mathbf{F}_{i+\frac{1}{2}} - \mathbf{F}_{i-\frac{1}{2}}] + \hat{\mathbf{S}}_i. \quad (5)$$

Here  $\hat{\mathbf{Q}}_i$  denotes the approximate cell average of the conserved variables in cell  $\Omega_i$  at time  $t$

$$\hat{\mathbf{Q}}_i(t) \approx \hat{\mathbf{q}}_i(t) = \frac{1}{\Delta x} \int_{\Omega_i} \mathbf{q}(x, t) dx, \quad (6)$$

where  $\hat{\mathbf{q}}_i(t)$  denotes the cell average of the exact solution  $\mathbf{q}(x, t)$ . In the following, a quantity with a hat  $\hat{\cdot}$  indicates a cell average and one without a hat indicates a point value. Note that this distinction is essential for higher-order methods of order greater than two. Likewise,  $\hat{\mathbf{S}}_i$  denotes the approximate cell average of the source terms at time  $t$

$$\hat{\mathbf{S}}_i(t) \approx \hat{\mathbf{s}}_i(t) = \frac{1}{\Delta x} \int_{\Omega_i} \mathbf{s}(\mathbf{q}(x, t), g(x)) dx, \quad (7)$$

where  $\hat{\mathbf{s}}_i(t)$  denotes the cell average of the exact source terms  $\mathbf{s}(\mathbf{q}, g)$ .

*Reconstruction* As the basic unknowns in the finite volume method are cell average values, we need some reconstruction procedure to recover the detailed spatial variation of the solution in order to obtain high order accuracy. The reconstruction procedure  $\mathcal{R}$  computes accurate point values of the approximate solution  $\mathbf{Q}_i(x, t)$  within cell  $\Omega_i$  from the cell averages  $\hat{\mathbf{Q}}_{i-k}, \dots, \hat{\mathbf{Q}}_i, \dots, \hat{\mathbf{Q}}_{i+k}$  ( $k > 0$ ) from a set of neighbouring cells, where the value of  $k$  depends on the desired order of accuracy. We denote a reconstruction procedure that recovers an  $m$ -th order accurate point value of the conserved variables at location  $x$  within cell  $\Omega_i$  from the cell averages by

$$\mathbf{Q}_i^{\text{rec}}(x) = \mathcal{R}\left(x; \left\{ \hat{\mathbf{Q}}_j \right\}_{j \in S_i}\right). \quad (8)$$

where  $S_i = \{i-k, \dots, i, \dots, i+k\}$  is the stencil of the reconstruction. The  $m$ -th order accuracy means that the error in the reconstructed value is of  $O(\Delta x^m)$ , or equivalently, the method can exactly reconstruct any polynomial of degree at most  $m-1$ .

Many such reconstruction procedures have been developed in the literature, and a non-exhaustive list includes the Total Variation Diminishing (TVD) and the Monotonic Upwind Scheme for Conservation Laws (MUSCL) methods (see e.g. [55, 25, 48, 34, 37, 50]), the Piecewise Parabolic Method (PPM) [17], the Essentially Non-Oscillatory (ENO) (see e.g. [24]), Weighted ENO (WENO) (see e.g. [47] and references therein) and Central WENO (CWENO) methods (see e.g. [18]).

In this paper, we will use the  $m$ -th order CWENO reconstructions [18] with  $m$  odd. A distinctive feature of CWENO reconstruction is that it provides an analytic expression for the reconstruction polynomial and not just a value at some particular point within the cell. In particular, for the numerical tests, we will use the third-order accurate CWENO3 from [32] and the fifth-order accurate CWENO5 from [8]. However, the schemes developed in this paper are not restricted to this choice of reconstruction schemes.

*Numerical flux* At each cell face, we have obtained two solution values from the reconstructions in the two surrounding cells. The flux

$$\mathbf{F}_{i+\frac{1}{2}} = \mathcal{F}\left(\mathbf{Q}_i^{\text{rec}}\left(x_{i+\frac{1}{2}}\right), \mathbf{Q}_{i+1}^{\text{rec}}\left(x_{i+\frac{1}{2}}\right)\right) \quad (9)$$

across the  $i + \frac{1}{2}$  face is obtained from a numerical flux formula  $\mathcal{F}$ , which is usually based on (approximately) solving Riemann problems at cell interfaces. The numerical flux function  $\mathcal{F}$  is required to be consistent, i.e.  $\mathcal{F}(\mathbf{Q}, \mathbf{Q}) = \mathbf{f}(\mathbf{Q})$  and Lipschitz continuous. Moreover, we will require that it satisfies the *contact property*:

**Definition 1 (Contact property)** Let  $\rho_L$  ( $\rho_R$ ) be the density on the left (right) side of a contact discontinuity and  $p$  the constant pressure. A numerical flux function  $\mathcal{F}$  for the one-dimensional Euler equations that satisfies the condition

$$\mathcal{F}(\mathbf{Q}(\rho_L, 0, p), \mathbf{Q}(\rho_R, 0, p)) = [0, p, 0]^T \quad (10)$$

is said to have the *contact property*. Here,  $\mathbf{Q} = \mathbf{Q}(\rho, u, p)$  denotes the transformation from primitive to conserved variables.

This property ensures the ability of a numerical flux to exactly capture stationary contact discontinuities of the Euler equations. In our tests below, we will use the well-known approximate Riemann solver by Roe [46]. Another well-known flux with the contact property is the HLLC flux [51]. The Rusanov flux is not able to capture contact discontinuities since it does not satisfy Definition 1. Note, that the contact property is -besides consistency- the only requirement for a numerical flux to use with the well-balanced methods proposed in this article. This gives a lot of freedom, since there are many contact property satisfying numerical fluxes with different properties available in literature. This includes for example entropy stable fluxes (e.g. [27, 14, 6]) and numerical fluxes suitable for the simulation of low Mach number flows (e.g. [54, 40, 41, 42, 2, 6])

*Source terms discretization* An accurate approximation of the cell average of the source terms is obtained by (numerical) integration:

$$\hat{\mathbf{S}}_i(t) = \frac{1}{\Delta x} \int_{\Omega_i} \mathbf{s}(\mathbf{Q}_i^{\text{rec}}(x, t), g(x)) \, dx \approx \frac{1}{\Delta x} \mathcal{Q}_i(\mathbf{s}(\mathbf{Q}_i^{\text{rec}}, g)) = \frac{1}{\Delta x} \sum_{\alpha=1}^{N_q} \omega_\alpha \mathbf{s}(\mathbf{Q}_i^{\text{rec}}(x_{i,\alpha}, t), g(x_{i,\alpha})), \quad (11)$$

where the  $x_{i,\alpha} \in \Omega_i$  and  $\omega_\alpha$  denote the  $N_q$  nodes and weights of a  $q$ -th order accurate quadrature rule  $\mathcal{Q}_i$ , respectively. The point values of the conserved variables are obtained from the reconstruction procedure Eq. (8). We assume here that the gravitational acceleration  $g(x)$  is either known analytically or obtained from a suitably accurate interpolation if it is only known discretely. In practice, we can choose the quadrature rule so that it can exactly integrate any polynomial of degree

at most  $m - 1$ , where  $m$  is the order of the reconstruction scheme. If the gravitational acceleration is approximated e.g. using an  $m$ -th order accurate CWENO interpolation, we evaluate the integral Eq. (11) analytically. This is computationally less expensive than using a quadrature rule.

*Time-stepping* For the temporal integration, the time domain of interest  $[0, T]$  is discretized into time steps  $\Delta t = t^{n+1} - t^n$ , where the superscripts label the different time levels. The semi-discrete scheme Eq. (5) is evolved in time using some ODE integrator. For this purpose, we apply explicit Runge–Kutta methods. To achieve third-order accuracy in time, we use a third-order accurate, four stage explicit Runge–Kutta method [33]. To achieve fifth-order accuracy in time, we apply a fifth-order accurate Runge–Kutta method (the standard-method from [45]). Furthermore, the time step  $\Delta t$  is required to fulfill a CFL condition for stability. We emphasize that implicit time integrators could also be used. Though, for our convenience, we only present results computed with the above explicit time integrators.

This concludes the description of a standard high-order accurate finite volume scheme. We refer to the many excellent available textbooks for further information and detailed derivation, see e.g. [34, 37, 26, 50]. However, a standard finite volume method is in general not able to exactly balance hydrostatic equilibrium solutions. Next, we present the necessary modifications to the reconstruction procedure, which render this precise balance possible and result in a family of high-order well-balanced schemes.

## 2.3 The discretely well-balanced method

### 2.3.1 Source term discretization

Let us define the source term approximation for the momentum and energy equations by

$$s_h^i(x) = -\rho_i^{\text{rec}}(x)g_i^{\text{int}}(x) \quad \text{and} \quad (us)_h^i(x) = -(\rho u)_i^{\text{rec}}(x)g_i^{\text{int}}(x)$$

for each cell and set

$$s_h(x) = s_h^i(x) \quad \text{and} \quad (us)_h(x) = (us)_h^i(x) \quad \text{for} \quad x \in [x_{i-\frac{1}{2}}, x_{i+\frac{1}{2}}],$$

where  $\rho_i^{\text{rec}}$  and  $(\rho u)_i^{\text{rec}}$  are the  $m$ -th order accurate CWENO reconstruction polynomials in the  $i$ -th cell.  $g_i^{\text{int}}$  has been interpolated from cell-centered point values using  $m$ -th order accurate polynomial interpolation. In that way, the source term  $s_h^i$  and  $(us)_h^i$  is uniquely defined on the whole domain. Note that source term integrals can be computed explicitly, since  $s_h$  and  $(us)_h$  are piecewise products of polynomials.

With these approximations, the cell-averaged source term used in the finite volume method in the  $i$ -th cell is computed from

$$\mathbf{s}_i := \begin{pmatrix} 0 \\ s_h(x) \\ (us)_h(x) \end{pmatrix}$$

as described in Eq. (11) using the exact integration.

*Remark 1* Note that any other high order source term approximation can be used in our algorithm, as long as it provides a function which is defined in the whole cell and that can be consistently extrapolated to neighboring cells.

### 2.3.2 Local hydrostatic reconstruction

The basic idea of the local hydrostatic reconstruction is to reconstruct deviations to a high order accurate local equilibrium profile  $\mathbf{Q}_i^{\text{eq}}(x)$  consistent with the cell-averaged conserved variables. To find a cell's equilibrium profile the source term is integrated to neighboring cells. This procedure will now be described in technical detail.

*Step 1* We begin by the construction of the high-order local equilibrium profile. A one-dimensional hydrostatic equilibrium is by definition given by the solution of the hydrostatic equation

$$\frac{dp^{\text{eq}}}{dx} = -\rho(x)g(x). \quad (12)$$

Note that the above equation only describes a mechanical equilibrium and no thermal equilibrium is explicitly implied. We build the local pressure equilibrium profile  $p_i^{\text{eq}}(x)$  within the  $i$ -th cell by simply integrating Eq. (12)

$$p_i^{\text{eq}}(x) = p_{0,i} + \int_{x_i}^x s_h(\xi) \, d\xi, \quad (13)$$

where  $p_{0,i}$  is the point value of the pressure at cell center  $x_i$ , and  $\rho_i^{\text{eq}}(x)$  the equilibrium density profile within cell  $\Omega_i$ .

The equilibrium internal energy density  $\varepsilon_i^{\text{eq}}(x)$  profile can be computed through the EoS:

$$\varepsilon_i^{\text{eq}}(x) = \varepsilon(\rho_i^{\text{eq}}(x), p_i^{\text{eq}}(x)). \quad (14)$$

For the equilibrium discretization we choose  $\rho^{\text{eq}} = \rho^{\text{rec}}$ . The computational cost of this computation depends strongly on the functional form of the EoS. In the ideal gas case, the computation is trivial and can be performed explicitly

$$\varepsilon_i^{\text{eq}}(x) = \frac{p_i^{\text{eq}}(x)}{\gamma - 1}. \quad (15)$$

The cell center pressure  $p_{0,i}$ , which anchors the equilibrium pressure profile Eq. (13) at cell center, is fixed by demanding that the equilibrium internal density profile is consistent up to the desired order of accuracy with the cell average of internal energy density  $\hat{\varepsilon}_i$  within cell  $\Omega_i$ :

$$\hat{\varepsilon}_i = \frac{1}{\Delta x} \int_{x_{i-\frac{1}{2}}}^{x_{i+\frac{1}{2}}} \varepsilon_i^{\text{eq}}(x) \, dx. \quad (16)$$

Here,  $\hat{\varepsilon}_i$  is an estimate of the cell-averaged internal energy density in cell  $\Omega_i$ . The latter is, following [23], estimated from the conserved variables as

$$\hat{\varepsilon}_i = \hat{E}_i - \frac{1}{2} \frac{\hat{\rho} \hat{u}_i^2}{\hat{\rho}_i}, \quad (17)$$

which is exact at equilibrium ( $u = 0$ ).

For general EoS, Eq. (16) is a scalar nonlinear equation for the cell center pressure  $p_{0,i}$ . The general case is discussed in Section 2.4.3.

In the ideal gas case, Eq. (16) is linear and can be solved explicitly to yield

$$p_{0,i} = (\gamma - 1)\hat{\varepsilon}_i + \frac{1}{\Delta x} \int_{x_{i-\frac{1}{2}}}^{x_{i+\frac{1}{2}}} \int_{x_i}^x s_h(\xi) \, d\xi \, dx. \quad (18)$$

Now that the pressure at cell center  $p_{0,i}$  is fixed, we have fully specified the high-order accurate representation of the equilibrium conserved variables in cell  $\Omega_i$ :

$$\mathbf{Q}_i^{\text{eq}}(x) = \begin{pmatrix} \rho_i^{\text{eq}}(x) \\ 0 \\ \varepsilon_i^{\text{eq}}(x) \end{pmatrix}. \quad (19)$$

Similarly, the equilibrium reconstruction of the primitive variables are given by

$$\mathbf{W}_i^{\text{eq}}(x) = \begin{pmatrix} \rho_i^{\text{eq}}(x) \\ 0 \\ p_i^{\text{eq}}(x) \end{pmatrix}. \quad (20)$$

We stress here that the equilibrium density reconstruction is simply the result provided by the standard reconstruction procedure  $\mathcal{R}$ , i.e.  $\rho_i^{\text{eq}}(x) = \rho_i^{\text{rec}}(x)$ .

*Step 2* Next, we develop the high-order equilibrium preserving reconstruction procedure. To this end, we follow e.g. [23,4] and decompose in every cell the solution into an equilibrium and a (not necessarily small) perturbation part. The equilibrium part in cell  $\Omega_i$  is simply given by  $\mathbf{Q}_i^{\text{eq}}(x)$  of Eq. (19). The perturbation part in cell  $\Omega_i$  is obtained by applying the standard reconstruction procedure  $\mathcal{R}$  to the cell-averaged equilibrium perturbation

$$\delta \mathbf{Q}_i^{\text{rec}}(x) = \mathcal{R}\left(x; \left\{ \delta \hat{\mathbf{Q}}_k \right\}_{k \in S_i}\right), \quad \delta \hat{\mathbf{Q}}_k = \hat{\mathbf{Q}}_k - \frac{1}{\Delta x} \int_{x_{k-\frac{1}{2}}}^{x_{k+\frac{1}{2}}} \mathbf{Q}_i^{\text{eq}}(\xi) d\xi \quad (21)$$

We note that the cell average of the equilibrium perturbation in cell  $\Omega_k$  is obtained by taking the difference between the cell average  $\hat{\mathbf{Q}}_k$  and the cell average  $\hat{\mathbf{Q}}_i^{\text{eq}}$  of the equilibrium in cell  $\Omega_k$ . The latter is obtained by integrating the equilibrium profile  $\mathbf{Q}_i^{\text{eq}}$  of cell  $\Omega_i$  over  $\Omega_k$ . It is clear, that this construction results in a  $\min(q, r)$ -th order accurate representation of the equilibrium perturbation in cell  $\Omega_i$ .

*Step 3* The complete equilibrium preserving reconstruction  $\mathcal{W}$  is obtained by the sum of the equilibrium and perturbation reconstruction

$$\mathbf{Q}_i^{\text{rec}}(x) = \mathcal{W}\left(x; \left\{ \hat{\mathbf{Q}}_k \right\}_{k \in S_i}\right) = \mathbf{Q}_i^{\text{eq}}(x) + \delta \mathbf{Q}_i^{\text{rec}}(x). \quad (22)$$

This concludes the description of the equilibrium preserving reconstruction procedure. Replacing only this component in a finite volume method renders it well-balanced for arbitrary hydrostatic equilibria, i.e., only a mechanical equilibrium and no thermal equilibrium needs to be explicitly assumed. In the rest of the article, we will refer to the method introduced in this section as discretely well-balanced (DWB) method.

### 2.3.3 Well-balanced property of the discretely well-balanced method

We summarize the well-balancing property of the DWB method in the following theorem.

**Theorem 2.1** *Consider the scheme (5) with a consistent, Lipschitz continuous, and contact property fulfilling (Definition 1) numerical flux  $\mathcal{F}$ , an  $m$ -th order accurate spatial reconstruction procedure  $\mathcal{R}$ , the hydrostatic reconstruction  $\mathcal{W}$  (Eq. (22)) and the gravitational source term (11).*

*This scheme has the following properties:*

- (i) *The scheme is at least  $\min(q, m)$ -th order accurate in space (for smooth solutions).*

(ii) For ideal gas, the scheme is well-balanced in the sense that it preserves the discrete hydrostatic equilibrium defined by

$$p_{0,i+1} - p_{0,i} = \int_{x_i}^{x_{i+1}} s_h(\xi) d\xi, \quad u_i = 0, \quad \forall i, \quad (23)$$

where  $p_{0,i+1}$  and  $p_{0,i}$  are computed as described in Eq. (18).

*Proof* (i) The overall accuracy of the scheme is determined by the accuracy of reconstruction ( $m$ ) and source term integration ( $q$ ), which is  $\min(q, m)$ .

(ii) Due to  $(\hat{\rho}u)_i = 0$  and Eq. (17) we have  $\hat{E}_i = \hat{\varepsilon}_i$ . Consistency of the reconstruction in Eqs. (21) and (22) ensures  $\delta E_i(x) = 0$  for all  $i$ . Using Eq. (23) we have

$$\begin{aligned} p_{i+1}^{\text{eq}}(x_{i+\frac{1}{2}}) &= p_{0,i+1} + \int_{x_{i+1}}^{x_{i+\frac{1}{2}}} s_h(\xi) d\xi = p_{0,i} + \int_{x_i}^{x_{i+1}} s_h(\xi) d\xi + \int_{x_{i+1}}^{x_{i+\frac{1}{2}}} s_h(\xi) d\xi = p_{0,i} + \int_{x_i}^x s_h(\xi) d\xi \\ &= p_i^{\text{eq}}(x_{i+\frac{1}{2}}). \end{aligned}$$

For an ideal gas this involves

$$E_{i+1}^{\text{rec}}(x_{i+\frac{1}{2}}) = \delta E_{i+1}(x_{i+\frac{1}{2}}) + \frac{p_{i+1}^{\text{eq}}(x_{i+\frac{1}{2}})}{\gamma - 1} = \delta E_i(x_{i+\frac{1}{2}}) + \frac{p_i^{\text{eq}}(x_{i+\frac{1}{2}})}{\gamma - 1} = E_i^{\text{rec}}(x_{i+\frac{1}{2}}).$$

For an ideal gas, hence also the interface pressure values coincide and take the value  $p_{i+\frac{1}{2}}^{L/R} = p_i^{\text{eq}}(x_{i+\frac{1}{2}})$ . Due to the contact property of the numerical flux we have

$$\frac{1}{\Delta x} \left( \left( \mathbf{F}_{i+\frac{1}{2}} \right)_{\rho u} - \left( \mathbf{F}_{i-\frac{1}{2}} \right)_{\rho u} \right) = \frac{1}{\Delta x} \left( p_i^{\text{eq}}(x_{i+\frac{1}{2}}) - p_i^{\text{eq}}(x_{i+\frac{1}{2}}) \right) = \frac{1}{\Delta x} \int_{x_{i-\frac{1}{2}}}^{x_{i+\frac{1}{2}}} s_h(x) dx = \left( \hat{\mathbf{S}}_i \right)_{\rho u}$$

in the momentum equation. Also, since the contact property holds and the corresponding conditions are met (same pressure on both interfaces, no velocity), the density and energy fluxes vanish following Definition 1.

### 2.3.4 Stencil of the discretely well-balanced method

As in the whole article, we will assume that the order of reconstruction  $m$  to be odd. To update the cell-average values  $\hat{\mathbf{Q}}_i$ , a standard  $m$ -th order method requires  $\hat{\mathbf{Q}}_{i-\frac{m+1}{2}}, \dots, \hat{\mathbf{Q}}_{i+\frac{m+1}{2}}$ . This includes  $\frac{m-1}{2}$  cells in each direction for the reconstruction and one for the flux computations from the reconstructed values in the  $i-1, i$ , and  $i+1$  cell.

The DWB increases the stencil in the following way: The transformation to local hydrostatic variables requires the values of  $s_h$  in each cell in the reconstruction stencil. This adds  $\frac{m-1}{2}$  cells in each direction to the stencil. In total, to update the cell-average values  $\hat{\mathbf{Q}}_i$ , the methods require the values  $\hat{\mathbf{Q}}_{i-m}, \dots, \hat{\mathbf{Q}}_{i+m}$ .

Depending on the application (especially in parallel computing using a domain decomposition), this increased stencil can lead to a considerable increase in computation time and memory. As a possible solution to this problem, we propose a modified method in the next section. This method only uses the stencil of the standard method.

## 2.4 The local approximation method

The reason for the increased stencil in the previous methods is that the source term has to be discretized in each cell of the CWENO stencil. To avoid this, we will now do the following: To compute the hydrostatic pressure with respect to the  $i$ -th cell, we only use the source term discretization from the  $i$ -th cell. This definition is extended to the whole domain in the trivial way without using additional information. Consequently, there is no unique source term discretization. Instead it depends on the cell in which we aim to reconstruct.

To achieve this, we only have to modify Eq. (13) in the well-balanced method by using  $s_h^i$  instead of  $s_h$ ; the local hydrostatic reconstruction of the pressure is given by

$$p_{eq,i}(x) = p_{0,i} - \int_{x_i}^x s_h^i(\xi) \, d\xi. \quad (24)$$

Thus, instead of using the globally defined source term approximation  $s_h$ , we extrapolate the source term polynomial from the  $i$ -th cell to the neighboring cells. This only effects the reconstruction of the energy deviations. The rest of the method remains unmodified. In the rest of the article, we refer to this modified method as local approximation (LA) method.

### 2.4.1 Stencil of the local approximation method

In the modified method, the reconstruction routine only requires the local hydrostatic pressure polynomial from the  $i$ -th cell. The stencil of the method is now the same as the stencil of the standard method of the same formal order of accuracy.

### 2.4.2 Well-balanced property of the local approximation method

For the LA method defined in Section 2.4, there is no globally defined hydrostatic pressure function. Consequently, in general there is no well-defined cell-to-cell relation like Eq. (23), which is balanced to machine precision. The relation only holds if the hydrostatic pressure polynomials in different cells can be described as one global polynomial.

Whether the LA methods actually succeeds in significantly reducing the discretization error at hydrostatic solutions has to be tested in numerical experiments.

### 2.4.3 The local approximation method for arbitrary EoS

In this section we extend our well-balanced methods to arbitrary EoS. In the description of our well-balanced methods we used the assumption of an ideal gas law. It is used in all places, in which there is an conversion between pressure and internal energy, i.e. in Eqs. (16) and (18). If a different EoS, which may not be explicitly solvable and highly nonlinear, is used, the cell averages of  $\varepsilon_{eq}$  have to be computed using a sufficiently accurate quadrature rule. Equation (16) can not be solved explicitly anymore to find  $p_0$ . Instead,  $p_0$  can be computed numerically, e.g. using Newton's method on Eq. (16). These methods will be referred to as discretely well-balanced method (iterative computation of  $p_0$ ) (DWB-EoS) and local approximation method (iterative computation of  $p_0$ ) (LA-EoS). However, since in each step of Newton's method a quadrature rule is applied we expect this approach to determine  $p_0$  to be computationally very expensive.

We propose the following simplification: Choose

$$\varepsilon_{0,i} := E_i^{\text{rec}}(x_i) - \frac{1}{2} \frac{((\rho u)_i^{\text{rec}}(x_i))^2}{\rho_i^{\text{rec}}(x_i)},$$

which is the cell-centered internal energy computed from the CWENO reconstruction polynomials. Then apply the EoS to compute

$$p_{0,i} := p_{\text{EoS}}(\rho_i^{\text{rec}}(x_i), \varepsilon_{0,i}).$$

The resulting methods will be referred to as discretely well-balanced method (fast computation of  $p_0$ ) (DWB-EoS) and local approximation method (fast computation of  $p_0$ ) (LA-EoS).

The methods DWB-EoS, DWB-EoS, LA-EoS, and LA-EoS can not satisfy a theorem like Theorem 2.1, however, we expect them to significantly improve the quality of numerical simulations close to hydrostatic states. The methods for general EoS will be applied in numerical tests in Sections 3.3.1 and 3.3.2.

### 3 Numerical experiments in one spatial dimension

In all numerical experiments in this section we use the standard Roe flux [46]. For the third order methods we use the third order accurate CWENO3 reconstruction proposed in [32] and the third-order accurate, four stage explicit Runge–Kutta method from [33]. For the fifth order accurate methods we use the fifth order accurate CWENO5 reconstruction proposed in [8] and the fifth order accurate standard Runge–Kutta method from [45].

#### 3.1 Isothermal hydrostatic solution

We consider an isothermal hydrostatic solution of the 1-d compressible Euler equations with gravitational source term and the ideal gas equation of state (we choose  $\gamma = 1.4$ ) given by

$$\tilde{\rho}(x) = \tilde{p}(x) = \exp(-\phi(x)), \quad \tilde{u} \equiv 0. \quad (25)$$

We set these initial conditions in the domain  $\Omega = [0, 1]$  for  $\phi(x) = -10x$  with Dirichlet boundary conditions and  $\phi(x) = \sin(2\pi x)$  with periodic boundary conditions. Dirichlet boundary conditions are realized via constant-in-time ghost-cells, which are initialized with the exact solution (i.e. Eq. (25) in this case). For this isothermal solution the speed of sound is  $c = \sqrt{\gamma p / \rho} = \sqrt{\gamma}$ . The sound crossing time is defined as

$$\tau := \int_{\Omega} \frac{1}{c} dx \quad (26)$$

which yields  $\tau = \sqrt{1/\gamma}$ . We run the test up to final time  $t = 2\tau \approx 1.7$ . Convergence rates for the standard method and the proposed well-balanced methods can be seen in Tables 1 and 2. The standard method shows convergence rates as expected. The well-balanced methods are not only more accurate than the standard method, they also show better convergence. Using the DWB method increases the order of accuracy by one order, using the LA method increases it by two orders.

The initial condition does not satisfy the discrete hydrostatic conditions in the theorem, so the errors are not zero. We now apply the DWB method to a slightly modified setup; we use the density given in Eq. (25) and integrate the internal energy such that it satisfies Eq. (23). This initial data are a third or fifth order accurate discretization of Eq. (25) respectively. The errors can be seen in Table 3. The DWB method maintains the discretized hydrostatic solution to machine precision. This is valid for the third as well as the fifth order methods.

Table 1:  $L^1$ -errors for an isothermal hydrostatic solution of the Euler equations after two sound crossing times computed using different methods. The setup is described in Section 3.1, the gravitational potential is  $\phi(x) = -10x$ .

<b>third order methods, <math>\phi(x) = -10x</math></b>							
method	N	$\rho$ error	$\rho$ rate	$\rho u$ error	$\rho u$ rate	$E$ error	$E$ rate
Standard	128	2.28e-05	—	5.25e-06	—	1.07e-04	—
	256	2.82e-06	3.0	6.54e-07	3.0	1.29e-05	3.0
	512	3.52e-07	3.0	8.21e-08	3.0	1.59e-06	3.0
DWB	128	1.10e-07	—	1.78e-08	—	2.03e-07	—
	256	6.62e-09	4.0	1.11e-09	4.0	1.23e-08	4.0
	512	4.09e-10	4.0	6.98e-11	4.0	7.60e-10	4.0
LA	128	3.69e-07	—	8.49e-08	—	1.65e-06	—
	256	1.11e-08	5.1	2.57e-09	5.0	4.95e-08	5.1
	512	3.28e-10	5.1	7.69e-11	5.1	1.42e-09	5.1
<b>fifth order methods, <math>\phi(x) = -10x</math></b>							
method	N	$\rho$ error	$\rho$ rate	$\rho u$ error	$\rho u$ rate	$E$ error	$E$ rate
Standard	128	7.20e-08	—	1.38e-08	—	3.19e-07	—
	256	2.24e-09	5.0	4.41e-10	5.0	1.01e-08	5.0
	512	6.97e-11	5.0	1.39e-11	5.0	3.14e-10	5.0
DWB	128	3.41e-10	—	3.92e-11	—	6.59e-10	—
	256	5.39e-12	6.0	6.86e-13	5.8	1.03e-11	6.0
	512	8.28e-14	6.0	1.10e-14	6.0	1.52e-13	6.1
LA	128	1.75e-10	—	3.72e-11	—	6.03e-10	—
	256	1.78e-12	6.6	3.84e-13	6.6	6.60e-12	6.5
	512	1.57e-14	6.8	3.52e-15	6.8	5.11e-14	7.0

Table 2:  $L^1$ -errors for an isothermal hydrostatic solution of the Euler equations after two sound crossing times computed using different methods. The setup is described in Section 3.1, the gravitational potential is  $\phi(x) = \sin(2\pi x)$ .

<b>third order methods, <math>\phi(x) = \sin(2\pi x)</math></b>							
method	N	$\rho$ error	$\rho$ rate	$\rho u$ error	$\rho u$ rate	$E$ error	$E$ rate
Standard	128	7.03e-05	—	7.89e-05	—	3.00e-04	—
	256	8.76e-06	3.0	1.13e-05	2.8	3.64e-05	3.0
	512	1.09e-06	3.0	1.54e-06	2.9	4.65e-06	3.0
DWB	128	4.53e-08	—	1.07e-07	—	1.48e-07	—
	256	2.79e-09	4.0	6.78e-09	4.0	9.14e-09	4.0
	512	1.69e-10	4.0	4.19e-10	4.0	5.55e-10	4.0
LA	128	2.66e-07	—	1.51e-07	—	7.02e-07	—
	256	8.70e-09	4.9	7.06e-09	4.4	2.50e-08	4.8
	512	2.68e-10	5.0	3.72e-10	4.2	9.14e-10	4.8
<b>fifth order methods, <math>\phi(x) = \sin(2\pi x)</math></b>							
method	N	$\rho$ error	$\rho$ rate	$\rho u$ error	$\rho u$ rate	$E$ error	$E$ rate
Standard	128	1.40e-07	—	9.10e-09	—	2.55e-07	—
	256	4.40e-09	5.0	3.10e-10	4.9	8.07e-09	5.0
	512	1.38e-10	5.0	1.02e-11	4.9	2.53e-10	5.0
DWB	128	1.64e-10	—	3.43e-10	—	5.45e-10	—
	256	2.60e-12	6.0	5.44e-12	6.0	8.61e-12	6.0
	512	9.24e-14	4.8	4.14e-14	7.0	2.01e-13	5.4
LA	128	2.75e-10	—	1.97e-10	—	5.15e-10	—
	256	1.78e-12	7.3	3.09e-12	6.0	4.36e-12	6.9
	512	8.19e-14	4.4	2.43e-14	7.0	2.17e-13	4.3

Table 3: balanced  $L^1$ -errors for an discrete isothermal hydrostatic solution of the Euler equations after time  $t = 2$  computed using different methods with a resolution of 128 cells. The initial data satisfy Eq. (23). The setup is described in Section 3.1.

Method	$\rho$ error	$\rho u$ error	$E$ error
Third order DWB	1.28e-16	7.64e-17	7.44e-16
Fifth order DWB	1.33e-16	1.57e-16	1.67e-16

Table 4:  $L^1$ -errors for the isothermal hydrostatic solution with perturbation  $\eta = 10^{-1}$  of the Euler equations after time  $t = 0.5$  computed using different methods. The setup is described in Section 3.2.

third order methods							
method	N	$\rho$ error	$\rho$ rate	$\rho u$ error	$\rho u$ rate	$E$ error	$E$ rate
Standard	128	1.67e-04	—	2.66e-04	—	5.73e-04	—
	256	3.02e-05	2.5	4.09e-05	2.7	9.78e-05	2.6
	512	5.51e-06	2.5	6.28e-06	2.7	1.73e-05	2.5
DWB	128	2.33e-04	—	2.55e-04	—	7.59e-04	—
	256	4.16e-05	2.5	4.29e-05	2.6	1.26e-04	2.6
	512	6.41e-06	2.7	6.10e-06	2.8	1.80e-05	2.8
LA	128	2.32e-04	—	2.54e-04	—	7.55e-04	—
	256	4.16e-05	2.5	4.28e-05	2.6	1.25e-04	2.6
	512	6.41e-06	2.7	6.10e-06	2.8	1.80e-05	2.8
fifth order methods, $\phi(x) = \sin(2\pi x)$							
method	N	$\rho$ error	$\rho$ rate	$\rho u$ error	$\rho u$ rate	$E$ error	$E$ rate
Standard	128	3.27e-06	—	3.83e-06	—	1.16e-05	—
	256	1.26e-07	4.7	1.50e-07	4.7	4.49e-07	4.7
	512	4.00e-09	5.0	4.81e-09	5.0	1.42e-08	5.0
DWB	128	4.49e-06	—	5.42e-06	—	1.59e-05	—
	256	1.78e-07	4.7	2.11e-07	4.7	6.33e-07	4.7
	512	6.18e-09	4.8	7.30e-09	4.9	2.20e-08	4.8
LA	128	4.49e-06	—	5.42e-06	—	1.59e-05	—
	256	1.78e-07	4.7	2.11e-07	4.7	6.33e-07	4.7
	512	6.18e-09	4.8	7.30e-09	4.9	2.20e-08	4.8

### 3.2 1-d hydrostatic solution with perturbation

Now we use the periodic potential  $\phi(x) = \sin(2\pi x)$  for the isothermal solution and add a perturbation

$$\rho(x) = \tilde{\rho}(x), \quad u(x) = \tilde{u}(x), \quad p(x) = \tilde{p}(x) + \eta \exp\left(-100\left(x - \frac{1}{2}\right)^2\right) \quad (27)$$

with  $\eta = 10^{-1}$ . We compute this test up to time  $t = 0.5$ . We compare the results with a simulation obtained from a seventh order standard method on a grid of 2024 cells. The errors and convergence rates of the standard and well-balanced methods are shown in Table 4. All methods show rates close to the expected rates for third and fifth order convergence, respectively. Next, to illustrate the capability of the well-balanced methods to capture small perturbations on the hydrostatic solution on a coarse grid, we use different grid sizes and methods for a perturbation amplitude of  $\eta = 10^{-5}$ . The result at time  $t = 0.5$  is shown in Figs. 1 and 2. The well-balanced methods succeed in resolving the perturbation significantly more accurately than the non-well-balanced standard method; the errors from the standard method are so large that they are not completely visible in the figures. The LA method is able to capture the small perturbations as accurately the DWB well-balanced method.

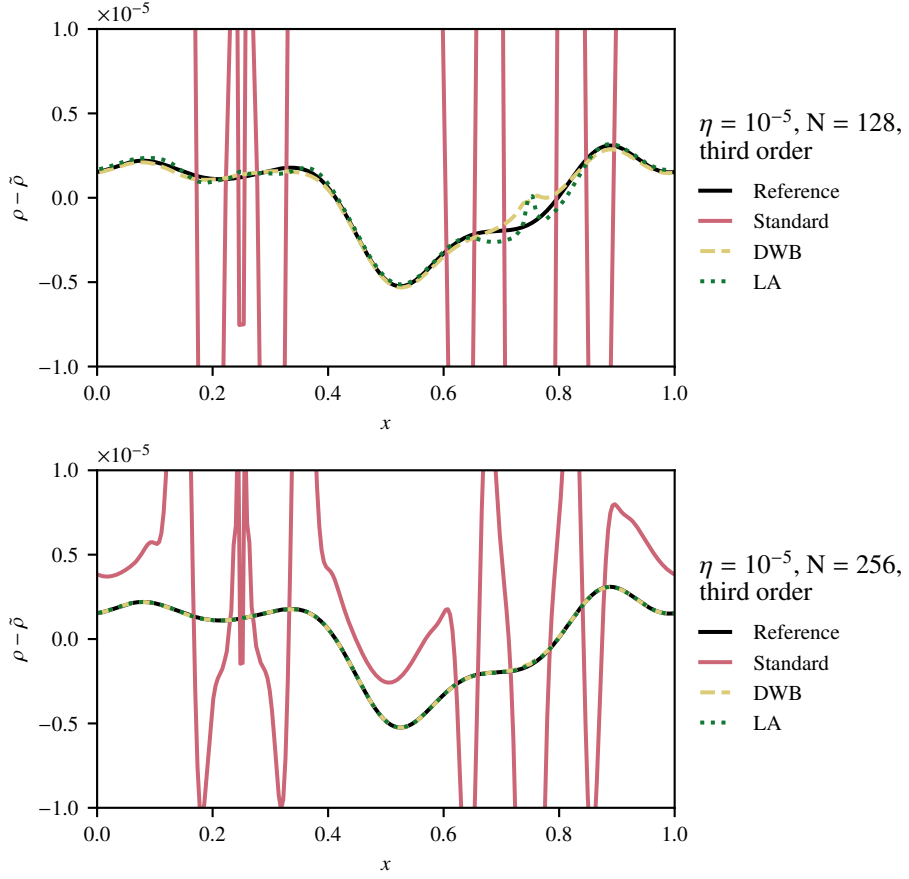


Fig. 1: Density deviation from the hydrostatic background for  $\eta = 10^{-5}$  using different grids at  $t = 0.5$ . Third order methods have been used. The test setup is described in Section 3.2.

### 3.3 Hydrostatic solution for an non-ideal gas equation of state

#### 3.3.1 Polytropic hydrostatic solution

Polytropic solutions of Eq. (1) are given by

$$\theta(x) := 1 - \frac{\nu - 1}{\nu} \phi(x), \quad \tilde{\rho}(x) = \theta(x)^{\frac{1}{\nu-1}}, \quad \tilde{p}(x) := \tilde{\rho}(x)^\nu, \quad (28)$$

and  $u = 0$ . Equation (28) describes a static state of the compressible Euler equations independent from the EoS. We choose the equation of state for an ideal gas which is additionally subject to radiation pressure [12]

$$p = \rho T + T^4, \quad (29)$$

where the temperature  $T$  is defined implicitly via

$$\varepsilon = \frac{\rho T}{\gamma - 1} + 3T^4. \quad (30)$$

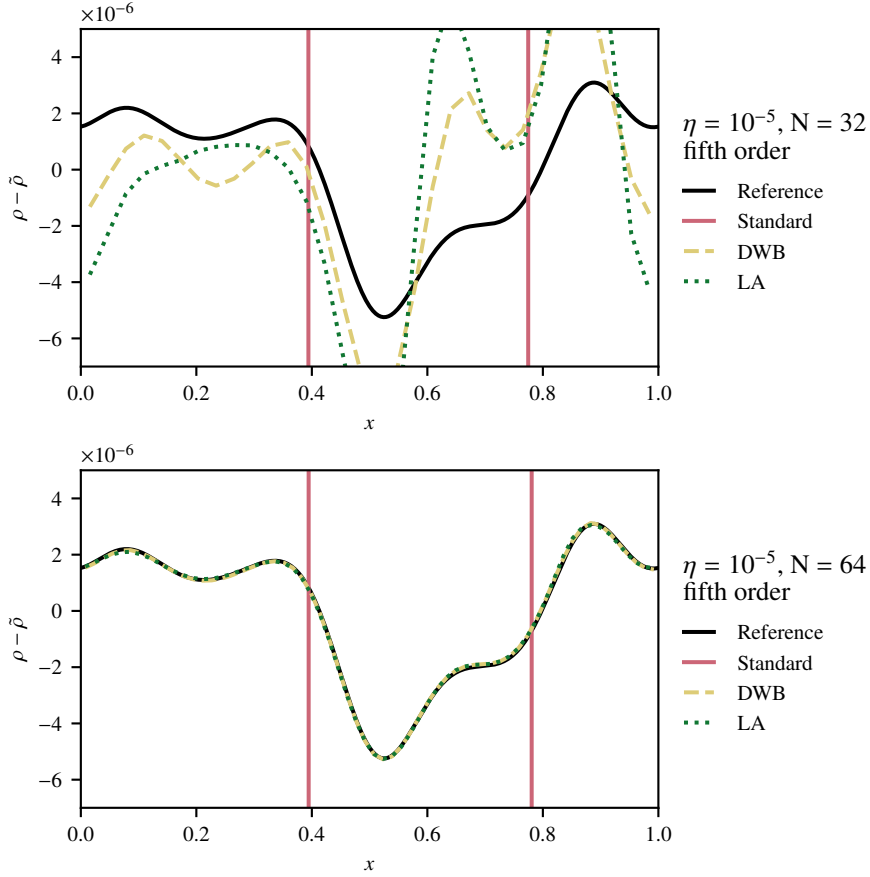


Fig. 2: Density deviation from the hydrostatic background for  $\eta = 10^{-5}$  using different grids at  $t = 0.5$ . Fifth order methods have been used. The test setup is described in Section 3.2.

The conversion between pressure  $p$  and internal energy density  $\varepsilon$  (while knowing the density  $\rho$ ) can not be computed explicitly. Instead, we use Newton's method to convert between  $p$  and  $\varepsilon$ . The speed of sound for this EoS can be computed by

$$c = \sqrt{\frac{\Gamma_1 p}{\rho}} \quad \text{where} \quad \Gamma_1 = \beta + \frac{(4 - 3\beta)^2(\gamma - 1)}{\beta + 12(\gamma - 1)(1 - \beta)} \quad \text{with} \quad \beta = \frac{\rho T}{p}. \quad (31)$$

The speed of sound is also computed using Newton's method. As for the ideal gas we use  $\gamma = 1.4$ . For the gravity potential we choose  $\phi(x) = gx$  with constant  $g = -1$ . The domain is  $\Omega = [0, 1]$  and Dirichlet boundary conditions are applied. The sound crossing time for this setup, computed from Eq. (26) and Eq. (31), is  $\tau \approx 0.7$ . We run the test to a final time of  $t = 10 \approx 14\tau$ . We use a standard method and the extensions of the DWB and LA methods for general EoS as described in Section 2.4.3. For the DWB method we use the iterative (DWB-EoS) and the fast (DWB-EoSf) computation of the cell-centered pressure. For the LA method we only use the fast computation (LA-EoSf), since the LA method it is an approximate well-balanced method anyway.

The  $L^1$ -errors and convergence rates of the tests are shown in Table 5. Using the well-balanced methods significantly reduces the errors (about one to two orders of magnitude). Note, that the difference between the two different versions of the DWB method is small. This justifies the usage

Table 5:  $L^1$ -errors and rates for the polytropic hydrostatic solution with an EoS for ideal gas with radiation pressure at time  $t = 10$  computed using different third order accurate methods. The setup is described in Section 3.3.1.

method	N	$\rho$ error	$\rho$ rate	$\rho u$ error	$\rho u$ rate	$E$ error	$E$ rate
Standard	16	8.24e-06	—	4.06e-06	—	1.01e-05	—
	32	1.17e-06	2.8	5.68e-07	2.8	1.10e-06	3.2
	64	1.64e-07	2.8	8.68e-08	2.7	1.08e-07	3.3
DWB-EoS	16	6.72e-07	—	6.74e-07	—	4.96e-07	—
	32	9.13e-08	2.9	9.24e-08	2.9	5.57e-08	3.2
	64	1.32e-08	2.8	1.35e-08	2.8	5.73e-09	3.3
DWB-EoSf	16	6.77e-07	—	6.93e-07	—	4.83e-07	—
	32	9.26e-08	2.9	9.48e-08	2.9	5.42e-08	3.2
	64	1.33e-08	2.8	1.38e-08	2.8	5.65e-09	3.3
LA-EoSf	16	3.55e-07	—	1.72e-07	—	4.27e-07	—
	32	5.03e-08	2.8	2.39e-08	2.8	4.71e-08	3.2
	64	7.01e-09	2.8	3.65e-09	2.7	4.69e-09	3.3

of the simplified and much faster computation of  $p_0$ . The LA-EoSf method performs best. For the general EoS we do not observe the increased order of convergence that was observed in Section 3.1 in the case of the ideal gas EoS.

### 3.3.2 Perturbation on a polytropic hydrostatic solution

Now we add a Gaussian perturbation to the hydrostatic solution and use the initial data

$$\rho(x) = \tilde{\rho}(x), \quad p(x) = \tilde{p}(x) + \eta \exp\left(-100(x - 0.3)^2\right),$$

and  $u = 0$  with  $\eta = 10^{-7}$ . We evolve those initial data to time  $t = 0.1$  with 128 grid cells resolution. Third order standard and well-balanced methods are applied. In the well-balanced methods we use the simplified way of computing the cell-centered pressure as described in Section 2.4.3 (DWB-EoSf, LA-EoSf). The result is shown in Fig. 3. The reference solution is computed using the seventh order accurate exactly well-balanced method from [4] on a grid of 2048 cells. Both well-balanced methods yield results much closer to the reference solution compared to the standard method. It gets evident that the approximate well-balanced methods can help resolving perturbations to hydrostatic states more accurately even with an equation of state different from ideal gas.

### 3.4 Riemann problem on an isothermal hydrostatic state

In the next test we use the initial data

$$\tilde{\rho}(x) := \begin{cases} ac \exp(-a\phi(x)) & \text{if } x < x_0, \\ b \exp(-b\phi(x)) & \text{if } x \geq x_0, \end{cases} \quad (32)$$

$$\tilde{p}(x) := \begin{cases} c \exp(-a\phi(x)) & \text{if } x < x_0, \\ \exp(-b\phi(x)) & \text{if } x \geq x_0. \end{cases} \quad (33)$$

Eqs. (32) to (33) describe a piecewise isothermal hydrostatic solution with a jump discontinuity at  $x = x_0$ , which gives rise to all three waves of the Euler equations; the parameters are chosen as  $x_0 = 0.125$ ,  $a = 0.5$ ,  $b = 1$ ,  $c = 2$ . An ideal gas EoS with  $\gamma = 1.4$  is applied. We set these initial data on the domain  $[0, 0.25]$  and evolve them to the final time  $t = 0.02$  using our third and fifth order methods on a grid with 128 cells and Dirichlet boundary conditions. Additionally we run the same tests using unlimited polynomial reconstruction and interpolation instead of CWENO reconstruction and

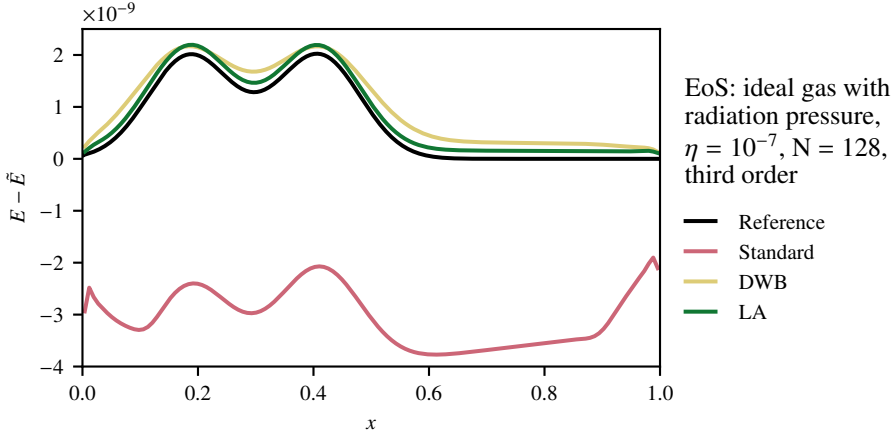


Fig. 3: Small perturbation ( $\eta = 10^{-7}$ ) on a polytropic hydrostatic solution with an EoS for ideal gas with radiation pressure after time  $t = 0.1$  computed using different third order accurate methods. The setup is described in Section 3.3.2. Energy perturbations  $E - \tilde{E}$  are shown.

interpolation. As a reference solution to compute the error we use a numerical solution obtained using a standard first order method with 32768 cells. In Fig. 4 we see the numerical results at final time for the LA methods. The simulations using unlimited polynomial reconstruction and interpolation introduce spurious oscillations. When CWENO limiting is used, no oscillations are visible. Using the DWB method leads to very similar results, hence we omit showing them for brevity.

To give quantitative results, we also compute the total variation of the solution at final time for all methods. The total variation of a quantity  $\alpha = \rho, \rho u, E$  of a numerical solution is defined by

$$\text{TV}(\alpha) := \sum_{i=1}^N |\alpha_i - \alpha_{i-1}|.$$

In Table 6 we present the difference in total variation relative to the total variation of the reference solution

$$\theta(\alpha) := \frac{\text{TV}(\alpha)}{\text{TV}(\alpha_{\text{ref}})} - 1. \quad (34)$$

A negative value of  $\theta$  indicates, that the total variation is smaller than in the reference solution. A positive value of  $\theta$  means that there are additional oscillations. In Table 6, the  $\theta$  values for different methods with and without CWENO limiting are presented alongside the  $L_1$  errors. All methods using CWENO limiting lead to a decrease in total variation in conserved variables. All unlimited methods introduce spurious oscillations.

## 4 Extension to two spatial dimensions

### 4.1 Two-dimensional compressible Euler equations with gravity

The two-dimensional compressible Euler equations which model the balance laws of mass, momentum, and energy under the influence of gravity are given by

$$\partial_t \mathbf{q} + \partial_x \mathbf{f} + \partial_y \mathbf{g} = \mathbf{s}, \quad (35)$$

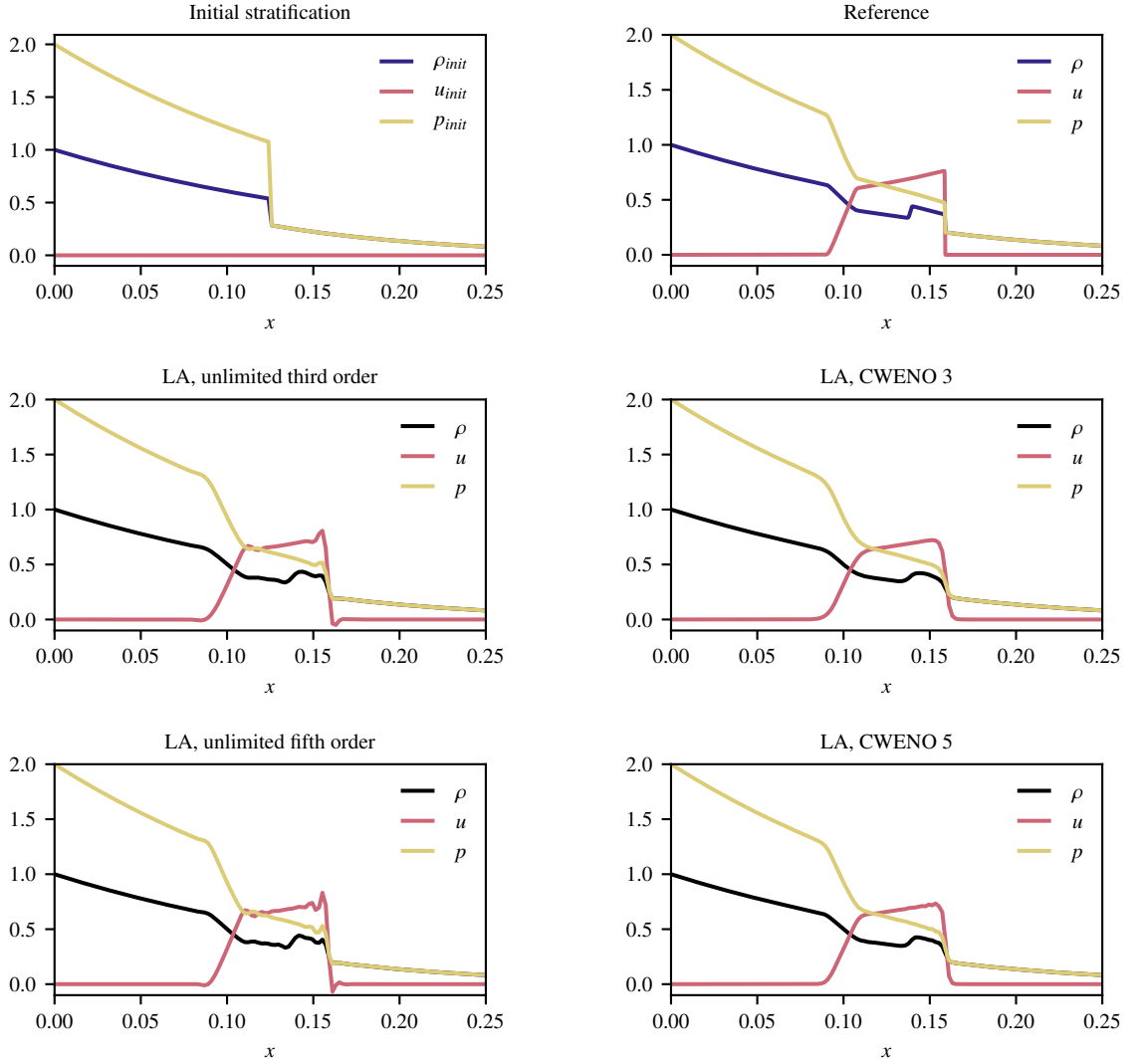


Fig. 4: Initial data (top left panel), reference solution (top right panel), and simulation results (all other panels) for the tests performed in Section 3.4. The formally third and fifth order LA methods are used with and without CWENO limiting.

where the conserved variables, fluxes and source terms are

$$\mathbf{q} = \begin{pmatrix} \rho \\ \rho u \\ \rho v \\ E \end{pmatrix}, \quad \mathbf{f} = \begin{pmatrix} \rho u \\ p + \rho u^2 \\ \rho uv \\ (E + p)u \end{pmatrix}, \quad \mathbf{g} = \begin{pmatrix} \rho v \\ \rho uv \\ p + \rho v^2 \\ (E + p)v \end{pmatrix}, \quad \mathbf{s} = \begin{pmatrix} 0 \\ -\rho g_x \\ -\rho g_y \\ -\rho u g_x - \rho v g_y \end{pmatrix} \quad (36)$$

with  $\rho, p > 0$ . Moreover,  $E = \varepsilon + \frac{1}{2}\rho|\mathbf{v}|^2$  is the total energy density with the velocity  $\mathbf{v} = (u, v)^T$  and specific internal energy  $e$ . The vector valued function  $\mathbf{x} \mapsto \mathbf{g}(\mathbf{x}) = (g_x(\mathbf{x}), g_y(\mathbf{x}))^T$  with  $\mathbf{x} := (x, y)^T$

Table 6: Errors and total variation for the robustness test from Section 3.4 at final time  $t = 0.02$ . The formally third and fifth order standard and well-balanced methods (DWB and dLA) are used with and without CWENO limiting. The oscillation indicator  $\theta$  is defined in Eq. (34).

third order methods						
method	$\rho$ error	$\theta(\rho)$	$\rho u$ error	$\theta(\rho u)$	$E$ error	$\theta(E)$
unlimited						
Standard	5.81e-04	2.50e-02	7.72e-04	2.30e-01	3.05e-03	4.70e-02
DWB	5.81e-04	2.50e-02	7.74e-04	2.31e-01	3.06e-03	4.72e-02
LA	5.81e-04	2.50e-02	7.74e-04	2.31e-01	3.06e-03	4.71e-02
CWENO 3						
Standard	6.51e-04	-4.18e-02	8.30e-04	-2.76e-02	3.25e-03	-5.73e-06
DWB	6.57e-04	-3.95e-02	8.33e-04	-2.70e-02	3.28e-03	-5.74e-06
LA	6.56e-04	-3.96e-02	8.33e-04	-2.70e-02	3.28e-03	-5.74e-06
fifth order methods						
method	$\rho$ error	$\theta(\rho)$	$\rho u$ error	$\theta(\rho u)$	$E$ error	$\theta(E)$
unlimited						
Standard	5.20e-04	1.10e-01	6.91e-04	4.67e-01	2.66e-03	1.20e-01
DWB	5.20e-04	1.10e-01	6.92e-04	4.68e-01	2.66e-03	1.20e-01
LA	5.20e-04	1.10e-01	6.92e-04	4.68e-01	2.66e-03	1.20e-01
CWENO 5						
Standard	5.00e-04	-3.67e-02	6.82e-04	-2.50e-02	2.79e-03	-5.74e-06
DWB	4.76e-04	-3.35e-02	6.48e-04	-2.35e-02	2.71e-03	-5.74e-06
LA	4.76e-04	-3.36e-02	6.47e-04	-2.38e-02	2.71e-03	-5.74e-06

is a given gravitational field. As in the one-dimensional case the system is closed using an EoS, which relates  $\rho$ ,  $p$ , and  $\varepsilon$ .

#### 4.2 Finite volume method in two spatial dimensions

We discretize the spatial domain  $\Omega := [x_{\min}, x_{\max}] \times [y_{\min}, y_{\max}]$  with  $x_{\min} < x_{\max}$  and  $y_{\min} < y_{\max}$  into  $N_x \times N_y$  finite control volumes  $\Omega_{ij} := [x_{i-\frac{1}{2}}, x_{i+\frac{1}{2}}] \times [y_{j-\frac{1}{2}}, y_{j+\frac{1}{2}}]$  for  $i = 1, \dots, N_x$  and  $j = 1, \dots, N_y$ . The interface positions in the  $x$  and  $y$ -direction are  $x_{i+\frac{1}{2}} := x_{\min} + i\Delta x$  and  $y_{j+\frac{1}{2}} := y_{\min} + j\Delta y$  with  $\Delta x = (x_{\max} - x_{\min})/N_x$ ,  $\Delta y = (y_{\max} - y_{\min})/N_y$  for  $i = 0, \dots, N_x$  and  $j = 0, \dots, N_y$ . The cell-centered coordinates are given by  $\mathbf{x}_{ij} = (x_i, y_j)^T = \left(\frac{1}{2}(x_{i-\frac{1}{2}} + x_{i+\frac{1}{2}}), \frac{1}{2}(y_{j-\frac{1}{2}} + y_{j+\frac{1}{2}})\right)$ . The compressible Euler equations with gravity (Eq. (35)) are integrated over each control volume and using some discretizations yields

$$\partial_t \hat{\mathbf{Q}}_{ij} = -\frac{1}{|\Omega_{ij}|} \left[ \mathbf{F}_{i+\frac{1}{2},j} - \mathbf{F}_{i-\frac{1}{2},j} + \mathbf{G}_{i,j+\frac{1}{2}} - \mathbf{G}_{i,j-\frac{1}{2}} \right] + \hat{\mathbf{S}}_{ij}, \quad (37)$$

where the interface fluxes are approximated by

$$\begin{aligned} \mathbf{F}_{i+\frac{1}{2},j} &:= \mathcal{Q}_{y \in [y_{j-\frac{1}{2}}, y_{j+\frac{1}{2}}]} \left( \mathcal{F} \left( \mathbf{Q}_{ij}^{\text{rec}} \left( x_{i+\frac{1}{2}}, y \right), \mathbf{Q}_{i+1,j}^{\text{rec}} \left( x_{i+\frac{1}{2}}, y \right) \right) \right) \approx \int_{y_{j-\frac{1}{2}}}^{y_{j+\frac{1}{2}}} \mathbf{f}(\mathbf{q}(x_{i+\frac{1}{2}}, y)) dy, \quad (38) \\ \mathbf{G}_{i,j+\frac{1}{2}} &:= \mathcal{Q}_{x \in [x_{i-\frac{1}{2}}, x_{i+\frac{1}{2}}]} \left( \mathcal{G} \left( \mathbf{Q}_{ij}^{\text{rec}} \left( x, y_{j+\frac{1}{2}} \right), \mathbf{Q}_{i,j+1}^{\text{rec}} \left( x, y_{j+\frac{1}{2}} \right) \right) \right) \approx \int_{x_{i-\frac{1}{2}}}^{x_{i+\frac{1}{2}}} \mathbf{g}(\mathbf{q}(x, y_{j+\frac{1}{2}})) dx. \end{aligned} \quad (39)$$

Here,  $\mathcal{Q}$  is an  $m$ -th order accurate quadrature rule,  $\mathcal{F}$  and  $\mathcal{G}$  are numerical fluxes as defined in Section 2.2, i.e. they are consistent, Lipschitz-continuous in both arguments, and they satisfy the contact

property. The reconstructed quantities  $\mathbf{Q}_{ij}^{\text{rec}}$  are obtained from an  $m$ -th order accurate reconstruction, i.e.

$$\mathbf{Q}_{ij}^{\text{rec}}(\mathbf{x}) := \mathcal{R}\left(\mathbf{x}, \left\{\hat{\mathbf{Q}}_{kl}\right\}_{(k,l) \in S_{ij}}\right),$$

where  $S_{ij}$  is the set of all index tuples of cells in the stencil of the reconstruction.  $\hat{\mathbf{S}}_{ij}$  is a consistent source term discretization. In practical application of the standard method (in Section 5) we use the source term discretization which is introduced later in Eq. (40). The semi-discrete scheme is evolved in time using a sufficiently high order accurate Runge–Kutta method.

#### 4.3 Discretely well-balanced method

In the tests of the one-dimensional methods, we saw that the method with reduced stencil (LA) converges better to hydrostatic states and gives more accurate results than the method with the large stencil (DWB). Also, in two spatial dimensions, a relation like Eq. (23) can not be easily defined for our polynomial approximation of the source term, since the curve integral is in general path-dependent, unless the gravitational field is parallel to grid lines. This rules out the formulation of a well-balanced theorem for a genuinely two-dimensional method. Since in multi-dimensional simulations, the compactness of the stencil is usually even more important, we only extend the LA method to two spatial dimensions. These methods will not be exactly well-balanced and the numerical experiments will show if they are useful in practice.

##### 4.3.1 Source term discretization

Let us define the source term approximation

$$\begin{aligned} \mathbf{s}_h^{ij}(\mathbf{x}) &:= \begin{pmatrix} s_{x,h}^{ij}(\mathbf{x}) \\ s_{y,h}^{ij}(\mathbf{x}) \end{pmatrix} := \begin{pmatrix} -\rho_{ij}^{\text{rec}}(\mathbf{x})(g_x)_{ij}^{\text{int}}(\mathbf{x}) \\ -\rho_{ij}^{\text{rec}}(\mathbf{x})(g_y)_{ij}^{\text{int}}(\mathbf{x}) \end{pmatrix}, \\ (\mathbf{v} \cdot \mathbf{s})_h^{ij}(\mathbf{x}) &:= -(\rho u)_{ij}^{\text{rec}}(\mathbf{x})(g_x)_{ij}^{\text{int}}(\mathbf{x}) - (\rho v)_{ij}^{\text{rec}}(\mathbf{x})(g_y)_{ij}^{\text{int}}(\mathbf{x}), \end{aligned}$$

where  $\rho_{ij}^{\text{rec}}$  and  $(\rho \mathbf{v})_{ij}^{\text{rec}} := ((\rho u)_{ij}^{\text{rec}}, (\rho v)_{ij}^{\text{rec}})^T$  are  $m$ -th order accurate CWENO reconstruction polynomials in the  $ij$ -th cell.  $\mathbf{g}_{ij}^{\text{int}}$  is an  $m$ -th order accurate interpolation polynomial from the cell-centered point values of  $\mathbf{g}$ . CWENO interpolation could be used if  $\mathbf{g}$  is not smooth. Note, that the statement from Remark 1 is also valid in the two-dimensional case. Due to the polynomial character of  $\mathbf{s}_h^{ij}$  and  $(\mathbf{v} \cdot \mathbf{s})_h^{ij}$  the source term integrals can be computed explicitly.

The cell-averaged source term used in the finite volume method in the  $i$ -th cell is hence computed as

$$\hat{\mathbf{S}}_{ij} := \frac{1}{|\Omega_{ij}|} \int_{\Omega_{ij}} \begin{pmatrix} 0 \\ s_{x,h}^{ij}(\mathbf{x}) \\ s_{y,h}^{ij}(\mathbf{x}) \\ (\mathbf{v} \cdot \mathbf{s})_h^{ij}(\mathbf{x}) \end{pmatrix} d\mathbf{x}. \quad (40)$$

##### 4.3.2 Reconstruction

We construct a local approximation to the hydrostatic pressure in the cell  $\Omega_{ij}$ . For that, we first define the local hydrostatic density  $\rho_{ij}^{\text{eq}} := \rho_{ij}^{\text{rec}}$ . To obtain the hydrostatic pressure, we use the approach

$$p_{ij}^{\text{eq}}(\mathbf{x}) := p_{ij}^0 + \int_0^1 \mathbf{s}_h^{ij}(\mathbf{x}_{ij} + (\mathbf{x} - \mathbf{x}_{ij})t) \cdot (\mathbf{x} - \mathbf{x}_{ij}) dt \quad (41)$$

for the approximation in the cell  $\Omega_{ij}$ . The cell-centered pressure value  $p_{ij}^0$  is determined by demanding

$$\frac{1}{|\Omega_{ij}|} \int_{\Omega_{ij}} \varepsilon_{ij}^{\text{eq}}(\mathbf{x}) d\mathbf{x} = \hat{\varepsilon}_{ij}, \quad (42)$$

where

$$\varepsilon_{ij}^{\text{eq}}(\mathbf{x}) := \varepsilon_{\text{EoS}}(\rho_{ij}^{\text{eq}}(\mathbf{x}), p_{ij}^{\text{eq}}(\mathbf{x}))$$

is defined via the EoS and the cell-averaged internal energy density is computed using

$$\hat{\varepsilon}_{ij} := \hat{E}_{ij} - \frac{(\hat{\rho}u)_{ij}^2 + (\hat{\rho}v)_{ij}^2}{2\hat{\rho}_{ij}}. \quad (43)$$

Note that the relation Eq. (43) is only second order accurate in general. However, on hydrostatic solutions it is exact since the momentum term vanishes in that case. Assuming an ideal gas, Eqs. (41) and (42) yield

$$p_{ij}^0 = (\gamma - 1)\hat{\varepsilon}_{ij} - \frac{1}{|\Omega_{ij}|} \int_{\Omega_{ij}} \int_0^1 \mathbf{s}_h(\mathbf{x}_{ij} + (\mathbf{x} - \mathbf{x}_{ij})t) \cdot (\mathbf{x} - \mathbf{x}_{ij}) dt d\mathbf{x}. \quad (44)$$

Now that the pressure at cell center  $p_{0,ij}$  is fixed, we have fully specified the high-order accurate representation of the equilibrium conserved variables in cell  $\Omega_{ij}$ :

$$\mathbf{Q}_{ij}^{\text{eq}}(\mathbf{x}) = \begin{pmatrix} \rho_{ij}^{\text{eq}}(\mathbf{x}) \\ 0 \\ 0 \\ \varepsilon_{ij}^{\text{eq}}(\mathbf{x}) \end{pmatrix}. \quad (45)$$

Similarly, the equilibrium reconstruction of the primitive variables are given by

$$\mathbf{W}_{ij}^{\text{eq}}(\mathbf{x}) = \begin{pmatrix} \rho_{ij}^{\text{eq}}(\mathbf{x}) \\ 0 \\ 0 \\ p_{ij}^{\text{eq}}(\mathbf{x}) \end{pmatrix}. \quad (46)$$

We stress here that the equilibrium density reconstruction is simply the result provided by the standard reconstruction procedure  $\mathcal{R}$ .

Next, we develop the high-order equilibrium preserving reconstruction procedure. To this end, as in e.g. [5,23], we decompose in every cell the solution into an equilibrium and a (possibly large) perturbation part. The equilibrium part in cell  $\Omega_{ij}$  is simply given by  $\mathbf{Q}_{ij}^{\text{eq}}(x)$  of Eq. (45) above. The perturbation part in cell  $\Omega_{ij}$  is obtained by applying the standard reconstruction procedure  $\mathcal{R}$  to the cell-averaged equilibrium perturbation

$$\delta\mathbf{Q}_{ij}(\mathbf{x}) = \mathcal{R}\left(\mathbf{x}; \left\{\delta\hat{\mathbf{Q}}_{kl}\right\}_{(k,l) \in S_{ij}}\right), \quad \delta\hat{\mathbf{Q}}_{kl} = \hat{\mathbf{Q}}_{kl} - \frac{1}{|\Omega_{ij}|} \int_{\Omega_{kl}} \mathbf{Q}_{ij}^{\text{eq}}(\boldsymbol{\xi}) d\boldsymbol{\xi} \quad (47)$$

We note that the cell average of the equilibrium perturbation in cell  $\Omega_{kl}$  is obtained by taking the difference between the cell average  $\hat{\mathbf{Q}}_{kl}$  and the cell average of the equilibrium  $\hat{\mathbf{Q}}_{ij}^{\text{eq}}$  in cell  $\Omega_{kl}$ .

The complete equilibrium preserving reconstruction  $\mathcal{W}$  is then obtained by the sum of the equilibrium and perturbation reconstruction

$$\mathbf{Q}_{ij}(\mathbf{x}) = \mathcal{W}\left(\mathbf{x}; \left\{\hat{\mathbf{Q}}_{kl}\right\}_{(k,l) \in S_{ij}}\right) = \mathbf{Q}_{ij}^{\text{eq}}(\mathbf{x}) + \delta\mathbf{Q}_{ij}(\mathbf{x}). \quad (48)$$

*Remark 2* The method can be applied for arbitrary EoS by extending the modifications from Section 2.4.3 to two spatial dimensions in a straight forward way.

*Remark 3* The approximate well-balanced method presented in this section can be extended to three spatial dimensions without further complications.

Table 7:  $L^1$ -errors for the 2-d polytrope described in Section 5.1.

method	N	$\rho$ error	$\rho$ rate	$\rho u$ error	$\rho u$ rate	$\rho v$ error	$\rho v$ rate	$E$ error	$E$ rate
Standard	32	1.40e-04	—	1.56e-05	—	1.56e-05	—	7.01e-05	—
	64	1.78e-05	3.0	1.92e-06	3.0	1.92e-06	3.0	8.79e-06	3.0
	128	2.24e-06	3.0	2.23e-07	3.1	2.23e-07	3.1	1.10e-06	3.0
LA	32	1.55e-07	—	1.57e-08	—	1.57e-08	—	9.58e-08	—
	64	5.04e-09	4.9	6.04e-10	4.7	6.04e-10	4.7	3.29e-09	4.9
	128	1.67e-10	4.9	2.39e-11	4.7	2.39e-11	4.7	1.21e-10	4.8

## 5 Numerical experiments in two spatial dimensions

In all numerical experiments in this section we use the standard Roe flux [46], Gauss-Legendre quadrature rules and the third order accurate CWENO3 reconstruction proposed in [39]. The semi-discrete schemes are evolved in time using a third-order accurate, four stage explicit Runge–Kutta method [33].

### 5.1 Two-dimensional polytrope

In this test, we apply our two-dimensional well-balanced method (LA) on a two-dimensional polytrope. A polytrope is a hydrostatic configuration of an adiabatic gaseous sphere held together by self-gravitation. The test setup is given by [23]

$$\tilde{\rho}(\mathbf{x}) := \frac{\sin(\sqrt{2\pi}|\mathbf{x}|)}{\sqrt{2\pi}|\mathbf{x}|}, \quad \tilde{p}(\mathbf{x}) := \tilde{\rho}(\mathbf{x})^\gamma, \quad \mathbf{g} := \nabla\phi(\mathbf{x}), \quad \phi(\mathbf{x}) := -2\frac{\sin(\sqrt{2\pi}|\mathbf{x}|)}{\sqrt{2\pi}|\mathbf{x}|}, \quad (49)$$

where we choose  $\gamma = 2$  and the functions  $\rho$  and  $\phi$  are extended to  $\mathbf{x} = 0$  continuously. We set these initial conditions on Cartesian meshes for the domain  $[-0.5, 0.5]^2$  and use our third order accurate standard and LA method on these initial data. We evolve them until time  $t = 5$ , which corresponds to approximately 6 sound crossing times. At the boundaries, we use Dirichlet boundary conditions. The resulting errors and convergence rates at different resolutions are presented in Table 7. Using the well-balanced method significantly reduces the error, even though the gravity is not aligned with a coordinate direction in this setup. Moreover, as in previous tests, the increased order of accuracy on the hydrostatic solution is observed for the LA method.

### 5.2 Perturbation on the two-dimensional polytrope

As in [23], we now add a perturbation to the polytrope to study if the application of our well-balanced methods can help resolving it more accurately. The initial pressure is perturbed in the following way

$$p_{\text{pert}}(\mathbf{x}) := \left(1 + A \exp\left(-\frac{|\mathbf{x}|^2}{0.05^2}\right)\right) \tilde{p}(\mathbf{x}).$$

In our tests, we use different amplitude of the perturbation corresponding to  $A = 10^{-2}, 10^{-6}, 10^{-8}$ . The spatial domain and numerical methods are the same as in Section 5.1. The final time is reduced to  $t = 0.2$ , such that the perturbation can not reach the boundary. As a reference solutions to compute the errors we use simulations on a  $256 \times 256$  grid obtained with the well-balanced method introduced in [5]. Since this well-balanced method is exact on the hydrostatic background, the solutions are accurate enough to use them as reference.  $L^1$  errors and convergence rates are presented in Table 8 which show that the LA method is better at resolving the smaller perturbations than the standard method. In Fig. 5 the pressure perturbation for the test with  $A = 10^{-8}$  on the  $128 \times 128$  grid is shown at final time, which again shows the benefits of the LA method over the standard method.

Table 8:  $L^1$ -errors and rates for perturbations of different size on the 2-d polytrope described in Section 5.2. The third order accurate standard and LA methods are used.

<b>Perturbation <math>A = 10^{-2}</math></b>									
method	N	$\rho$ error	$\rho$ rate	$\rho u$ error	$\rho u$ rate	$\rho v$ error	$\rho v$ rate	$E$ error	$E$ rate
Standard	32	5.27e-05	–	4.20e-05	–	4.20e-05	–	9.11e-05	–
	64	1.61e-05	1.7	1.32e-05	1.7	1.32e-05	1.7	2.86e-05	1.7
	128	2.53e-06	2.7	2.07e-06	2.7	2.07e-06	2.7	4.52e-06	2.7
LA	32	5.63e-05	–	4.87e-05	–	4.87e-05	–	1.03e-04	–
	64	2.07e-05	1.4	1.80e-05	1.4	1.80e-05	1.4	3.78e-05	1.4
	128	3.68e-06	2.5	3.21e-06	2.5	3.21e-06	2.5	6.73e-06	2.5
<b>Perturbation <math>A = 10^{-6}</math></b>									
method	N	$\rho$ error	$\rho$ rate	$\rho u$ error	$\rho u$ rate	$\rho v$ error	$\rho v$ rate	$E$ error	$E$ rate
Standard	32	1.52e-05	–	5.40e-06	–	5.40e-06	–	2.00e-05	–
	64	1.97e-06	2.9	6.67e-07	3.0	6.67e-07	3.0	2.60e-06	2.9
	128	2.50e-07	3.0	8.27e-08	3.0	8.27e-08	3.0	3.31e-07	3.0
LA	32	2.05e-08	–	7.33e-09	–	7.33e-09	–	2.91e-08	–
	64	2.39e-09	3.1	1.86e-09	2.0	1.86e-09	2.0	4.16e-09	2.8
	128	3.77e-10	2.7	3.25e-10	2.5	3.25e-10	2.5	6.84e-10	2.6
<b>Perturbation <math>A = 10^{-8}</math></b>									
method	N	$\rho$ error	$\rho$ rate	$\rho u$ error	$\rho u$ rate	$\rho v$ error	$\rho v$ rate	$E$ error	$E$ rate
Standard	32	1.52e-05	–	5.40e-06	–	5.40e-06	–	2.00e-05	–
	64	1.97e-06	2.9	6.67e-07	3.0	6.67e-07	3.0	2.60e-06	2.9
	128	2.50e-07	3.0	8.27e-08	3.0	8.27e-08	3.0	3.31e-07	3.0
LA	32	2.05e-08	–	5.13e-09	–	5.13e-09	–	2.91e-08	–
	64	6.80e-10	4.9	2.45e-10	4.4	2.45e-10	4.4	1.00e-09	4.9
	128	2.31e-11	4.9	1.51e-11	4.0	1.51e-11	4.0	3.62e-11	4.8

### 5.3 Radial Rayleigh–Taylor Instability

In this test, we use a piece-wise isothermal hydrostatic state in the two-dimensional gravitational potential

$$\phi(\mathbf{x}) := -20 \frac{\sin(\sqrt{2\pi} |\mathbf{x}|)}{\sqrt{2\pi} |\mathbf{x}|}$$

and gravitational acceleration  $\mathbf{g} := \nabla \phi(\mathbf{x})$ . The initial data are given by

$$(\rho, p)(\mathbf{x}) := \begin{cases} (\tilde{\rho}_{\text{in}}, \tilde{p}_{\text{in}})(\mathbf{x}) & \text{if } \|\mathbf{x}\|_2 < r_0, \\ (\tilde{\rho}_{\text{out}}, \tilde{p}_{\text{out}})(\mathbf{x}) & \text{else,} \end{cases} \quad \mathbf{v}(\mathbf{x}) := \begin{pmatrix} 0 \\ 0 \end{pmatrix},$$

where

$$\begin{aligned} \tilde{\rho}_{\text{in}}(\mathbf{x}) &:= a c \exp(-a \phi(\mathbf{x})), & \tilde{\rho}_{\text{out}}(\mathbf{x}) &:= b \exp(-b \phi(\mathbf{x})), \\ \tilde{p}_{\text{in}}(\mathbf{x}) &:= c \exp(-a \phi(\mathbf{x})), & \tilde{p}_{\text{out}}(\mathbf{x}) &:= \exp(-b \phi(\mathbf{x})), \end{aligned}$$

and  $c = \exp((a - b)\phi((r_0, 0)^T))$ . Choosing  $b > a$  makes the system unstable, such that Raleigh–Taylor instabilities are expected to develop [13].

For the numerical computations, we use the above initial data with  $r_0 = 0.2$  and  $(a, b) = (1, 2)$  in the domain  $[0, 0.5]^2$ , and evolve them until time  $t = 0.6$ . We use the third order accurate standard and LA method on a  $64 \times 64$  cells grid. At the  $x = 0$  and  $y = 0$  boundaries we use wall-boundary conditions which are consistent with the symmetry of the problem. At the outer boundaries we extrapolate  $(\rho - \tilde{\rho}_{\text{out}}, \rho u, \rho v, E - (\gamma - 1)\tilde{p}_{\text{out}})^T$  in order to not destroy the hydrostatic solution at the boundary. The results are visualized in Figs. 6 and 7. The simulation with the standard method

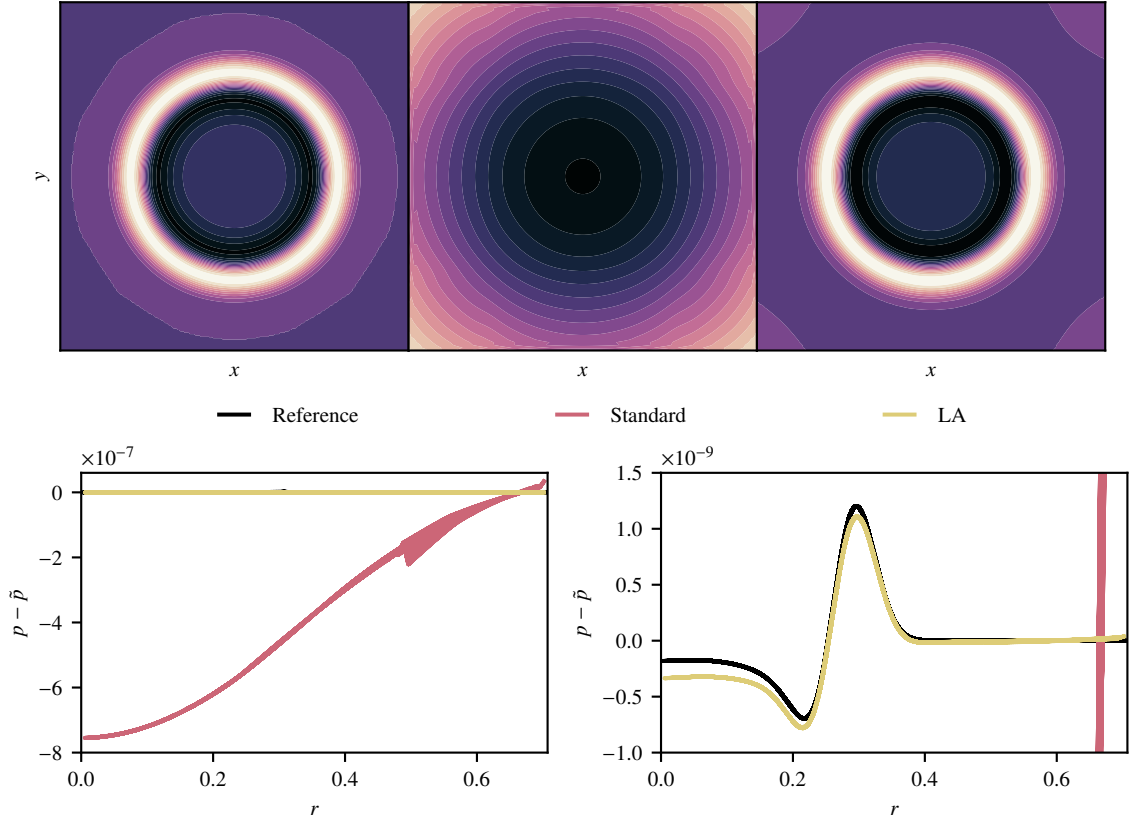


Fig. 5: Pressure perturbation  $p - \tilde{p}$  from the 2-d polytrope for the initial perturbation with  $A = 10^{-8}$  on a  $128 \times 128$  cells grid after time  $t = 0.2$ . The test is described in Section 5.2. The reference solution is obtained using the well-balanced method from [5] on a  $256 \times 256$  cells grid. In the top panels, the color ranges (dark to light) from  $-0.8e-8$  to  $1.2e-9$  in the left and right plot (reference and LA method) and from  $-8e-7$  to  $1e-7$  in the central plot (standard method). The full domain  $[-0.5, 0.5]^2$  is shown. The bottom panels show the pressure perturbation over radius in a scatter plot. The difference between the two bottom panels is the range of the values at the  $y$ -axis.

crashes approximately at time  $t \approx 0.2981$ . In Fig. 7 the relative density deviations  $\rho/\tilde{\rho}_{\text{initial}} - 1$  from the initial density over radius are shown at time  $t = 0.298$ . While the LA method is capable of accurately maintaining the hydrostatic solution away from the discontinuity, there are significant spurious perturbations for the standard method, especially at the outer boundary. In Fig. 6, the relative density deviation  $\rho/\tilde{\rho}_{\text{out}}$  is presented at different times. As expected, Rayleigh–Taylor instabilities appear at the interface between the light and the dense fluid.

## 6 Conclusions and Outlook

Novel well-balanced finite volume methods have been introduced. The first method (DWB method) exactly balances a high order discretization of any hydrostatic state exactly. However, it is restricted to the one-dimensional Euler system with gravity closed by an ideal gas law. Also, the stencil of the method is larger than the stencil of a standard method with the same order of accuracy. Localizing

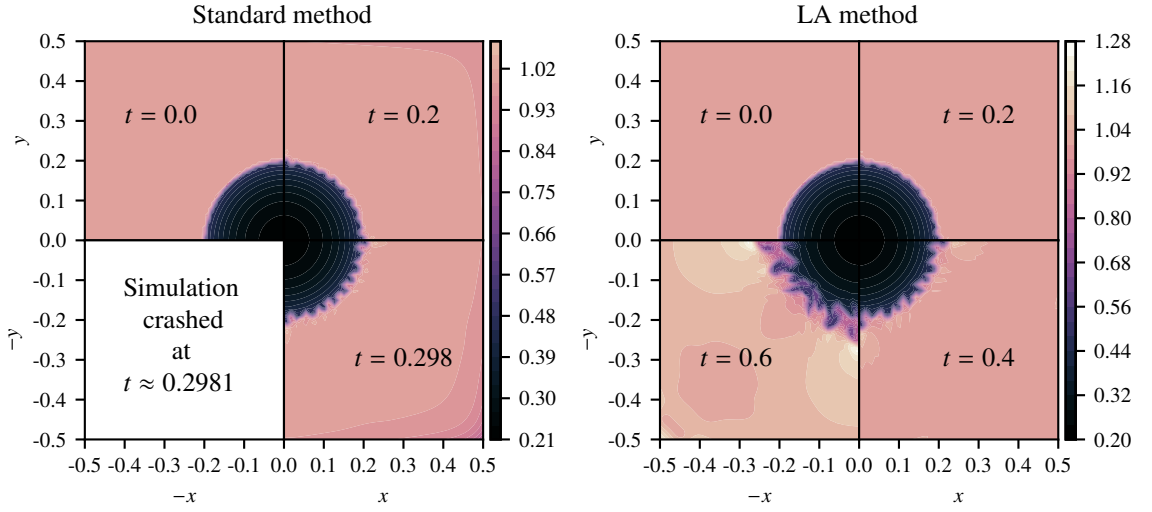


Fig. 6: Relative density deviation  $\rho/\tilde{\rho}_{\text{out}}$  from the outer hydrostatic state of the radial Rayleigh–Taylor instability. Setup and method are described in Section 5.3. Different times using the standard (left) and the LA method (right). The simulation using the standard method crashes at  $t \approx 0.2981$ .

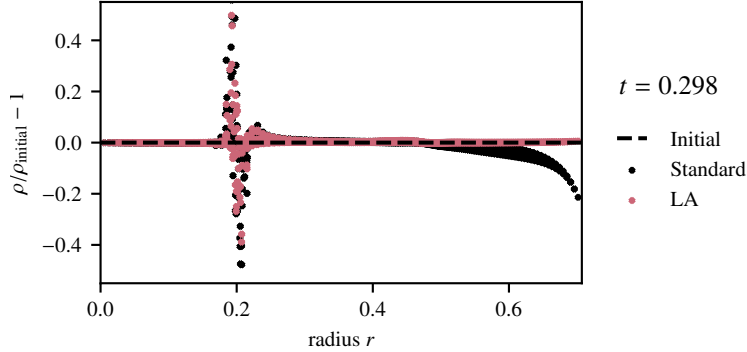


Fig. 7: Relative density deviations  $\rho/\tilde{\rho}_{\text{initial}} - 1$  from the initial density stratification over radius at time  $t = 0.298$  for the standard and LA method. The simulation using the standard method crashes at  $t \approx 0.2981$ .

the high order approximation to the hydrostatic state in each cell (LA method) reduced the stencil to the one of a comparable standard method. For the LA method the well-balanced property can not be shown analytically. However, in numerical tests it is found to be even more accurate on exact hydrostatic solutions than the DWB method. The LA method increased the order of accuracy for convergence towards hydrostatic states by two. This was observed not only in one spatial dimension but also in the two-dimensional extension. The LA method has been extended to arbitrary equations of state. The high order accuracy and the robustness of the DWB and LA method have been shown numerically. Also, numerical tests verified the capability of the methods to accurately capture small perturbations on hydrostatic states.

We conclude that the proposed well-balanced methods, in particular the LA method, are especially useful in situations, in which no knowledge about the structure of the hydrostatic states, which

will appear in the simulation, is available. It can be implemented in an existing code and can be used as the default method which significantly improves the accuracy at any hydrostatic state.

In further work, an extension of the method to more general grid systems, e.g. curvilinear grids, can be developed to make the method even more utilisable.

## References

1. Audusse, E., Bouchut, F., Bristeau, M.O., Klein, R., Perthame, B.: A fast and stable well-balanced scheme with hydrostatic reconstruction for shallow water flows. *SIAM Journal on Scientific Computing* **25**(6), 2050–2065 (2004)
2. Barsukow, W., Edelmann, P.V.F., Klingenberg, C., Miczek, F., Röpke, F.K.: A numerical scheme for the compressible low-mach number regime of ideal fluid dynamics. *Journal of Scientific Computing* pp. 1–24 (2017). DOI 10.1007/s10915-017-0372-4
3. Berberich, J.P., Chandrashekar, P., Klingenberg, C.: A general well-balanced finite volume scheme for euler equations with gravity. In: C. Klingenberg, M. Westdickenberg (eds.) *Theory, Numerics and Applications of Hyperbolic Problems I*, Springer Proceedings in Mathematics & Statistics 236, pp. 151–163 (2018)
4. Berberich, J.P., Chandrashekar, P., Klingenberg, C.: High order well-balanced finite volume methods for multi-dimensional systems of hyperbolic balance laws. *arXiv preprint arXiv:1903.05154* (2019)
5. Berberich, J.P., Chandrashekar, P., Klingenberg, C., Röpke, F.K.: Second order finite volume scheme for euler equations with gravity which is well-balanced for general equations of state and grid systems. *Communications in Computational Physics* **26**, 599–630 (2019)
6. Berberich, J.P., Klingenberg, C.: Entropy stable numerical fluxes for compressible euler equations which are suitable for all mach numbers. Accepted for publication in: *SEMA SIMAI Series: Numerical methods for hyperbolic problems Numhyp 2019* (2020)
7. Bermudez, A., Vázquez, M.E.: Upwind methods for hyperbolic conservation laws with source terms. *Computers & Fluids* **23**(8), 1049–1071 (1994)
8. Capdeville, G.: A central weno scheme for solving hyperbolic conservation laws on non-uniform meshes. *Journal of Computational Physics* **227**(5), 2977–3014 (2008)
9. Cargo, P., LeRoux, A.: A well balanced scheme for a model of atmosphere with gravity. *COMPOTES RENDUS DE L ACADEMIE DES SCIENCES SERIE I-MATHEMATIQUE* **318**(1), 73–76 (1994)
10. Castro, M.J., Parés, C.: Well-balanced high-order finite volume methods for systems of balance laws. *Journal of Scientific Computing* **82**(2), 48 (2020)
11. Castro, M.J., Semplice, M.: Third-and fourth-order well-balanced schemes for the shallow water equations based on the cwno reconstruction. *International Journal for Numerical Methods in Fluids* (2018)
12. Chandrasekhar, S.: An introduction to the study of stellar structure, vol. 2. Courier Corporation (1958)
13. Chandrasekhar, S.: *Hydrodynamic and Hydromagnetic Stability*. Clarendon Press, Oxford (1961)
14. Chandrashekar, P.: Kinetic energy preserving and entropy stable finite volume schemes for compressible euler and navier-stokes equations. *Communications in Computational Physics* **14**(5), 1252–1286 (2013)
15. Chandrashekar, P., Klingenberg, C.: A second order well-balanced finite volume scheme for euler equations with gravity. *SIAM Journal on Scientific Computing* **37**(3), B382–B402 (2015)
16. Chertock, A., Cui, S., Kurganov, A., Özcan, Ş.N., Tadmor, E.: Well-balanced schemes for the euler equations with gravitation: Conservative formulation using global fluxes. *Journal of Computational Physics* (2018)
17. Colella, P., Woodward, P.R.: The Piecewise Parabolic Method (PPM) for gas-dynamical simulations. *Journal of Computational Physics* **54**, 174–201 (1984)
18. Cravero, I., Puppo, G., Semplice, M., Visconti, G.: Cwno: uniformly accurate reconstructions for balance laws. *Mathematics of Computation* **87**(312), 1689–1719 (2018)
19. Desveaux, V., Zenk, M., Berthon, C., Klingenberg, C.: A well-balanced scheme for the euler equation with a gravitational potential. In: *Finite Volumes for Complex Applications VII-Methods and Theoretical Aspects*, pp. 217–226. Springer (2014)
20. Desveaux, V., Zenk, M., Berthon, C., Klingenberg, C.: A well-balanced scheme to capture non-explicit steady states in the euler equations with gravity. *International Journal for Numerical Methods in Fluids* **81**(2), 104–127 (2016)
21. Desveaux, V., Zenk, M., Berthon, C., Klingenberg, C.: Well-balanced schemes to capture non-explicit steady states: Ripa model. *Mathematics of Computation* **85**(300), 1571–1602 (2016)
22. Ghosh, D., Constantinescu, E.M.: Well-balanced, conservative finite difference algorithm for atmospheric flows. *AIAA Journal* (2016)
23. Grosheintz-Laval, L., Käppeli, R.: High-order well-balanced finite volume schemes for the euler equations with gravitation. *Journal of Computational Physics* **378**, 324–343 (2019)
24. Harten, A., Engquist, B., Osher, S., Chakravarthy, S.R.: Uniformly high order accurate essentially non-oscillatory schemes, iii. In: *Upwind and high-resolution schemes*, pp. 218–290. Springer (1987)

25. Harten, A., Lax, P.D., Van Leer, B.: On upstream differencing and godunov-type schemes for hyperbolic conservation laws. *SIAM Review* **25**, 35–61 (1983)
26. Hirsch, C.: Numerical computation of internal and external flows: The fundamentals of computational fluid dynamics. Butterworth-Heinemann (2007)
27. Ismail, F., Roe, P.L.: Affordable, entropy-consistent euler flux functions ii: Entropy production at shocks. *Journal of Computational Physics* **228**(15), 5410–5436 (2009)
28. Kanbar, F., Klingenberg, C., Touma, R.: Well-balanced central schemes for the one and two-dimensional euler systems with gravity. submitted to *Applied Numerical Mathematics* (2020)
29. Käppeli, R., Mishra, S.: Well-balanced schemes for the euler equations with gravitation. *Journal of Computational Physics* **259**, 199–219 (2014)
30. Käppeli, R., Mishra, S.: A well-balanced finite volume scheme for the euler equations with gravitation-the exact preservation of hydrostatic equilibrium with arbitrary entropy stratification. *Astronomy & Astrophysics* **587**, A94 (2016)
31. Klingenberg, C., Puppo, G., Semplice, M.: Arbitrary order finite volume well-balanced schemes for the euler equations with gravity. *SIAM Journal on Scientific Computing* **41**(2), A695–A721 (2019)
32. Kolb, O.: On the full and global accuracy of a compact third order weno scheme. *SIAM Journal on Numerical Analysis* **52**(5), 2335–2355 (2014)
33. Kraaijevanger, J.F.B.M.: Contractivity of runge-kutta methods. *BIT Numerical Mathematics* **31**(3), 482–528 (1991)
34. Laney, C.B.: Computational gasdynamics. Cambridge university press (1998)
35. LeVeque, R., Bale, D.: Wave propagation methods for conservation laws with source terms. Birkhauser Basel pp. 609–618 (1999)
36. LeVeque, R.J.: Balancing source terms and flux gradients in high-resolution godunov methods: the quasi-steady wave-propagation algorithm. *Journal of computational physics* **146**(1), 346–365 (1998)
37. LeVeque, R.J.: Finite volume methods for hyperbolic problems, vol. 31. Cambridge university press (2002)
38. LeVeque, R.J., George, D.L., Berger, M.J.: Tsunami modelling with adaptively refined finite volume methods. *Acta Numerica* **20**, 211–289 (2011)
39. Levy, D., Puppo, G., Russo, G.: A third order central weno scheme for 2d conservation laws. *Applied Numerical Mathematics* **33**(1), 415–422 (2000)
40. Li, X.s., Gu, C.w.: An all-speed roe-type scheme and its asymptotic analysis of low mach number behaviour. *Journal of Computational Physics* **227**(10), 5144–5159 (2008)
41. Li, X.s., Gu, C.w.: Mechanism of roe-type schemes for all-speed flows and its application. *Computers & Fluids* **86**, 56–70 (2013)
42. Miczek, F., Röpke, F.K., Edelmann, P.V.F.: New numerical solver for flows at various mach numbers. *Astronomy & Astrophysics Review* **576**, A50 (2015). DOI 10.1051/0004-6361/201425059
43. Noelle, S., Pankratz, N., Puppo, G., Natvig, J.R.: Well-balanced finite volume schemes of arbitrary order of accuracy for shallow water flows. *Journal of Computational Physics* **213**(2), 474–499 (2006)
44. Noelle, S., Xing, Y., Shu, C.W.: High-order well-balanced finite volume weno schemes for shallow water equation with moving water. *Journal of Computational Physics* **226**(1), 29–58 (2007)
45. Rabiei, F., Ismail, F.: Fifth-order improved runge-kutta method for solving ordinary differential equation. *Australian Journal of Basic and Applied Sciences* **6**(3), 97–105 (2012)
46. Roe, P.L.: Approximate riemann solvers, parameter vectors, and difference schemes. *Journal of Computational Physics* **43**(2), 357 – 372 (1981). DOI 10.1016/0021-9991(81)90128-5
47. Shu, C.W.: High order weighted essentially nonoscillatory schemes for convection dominated problems. *SIAM review* **51**(1), 82–126 (2009)
48. Sweby, P.K.: High resolution schemes using flux limiters for hyperbolic conservation laws. *SIAM journal on numerical analysis* **21**(5), 995–1011 (1984)
49. Thomann, A., Zenk, M., Klingenberg, C.: A second-order positivity-preserving well-balanced finite volume scheme for euler equations with gravity for arbitrary hydrostatic equilibria. *International Journal for Numerical Methods in Fluids* **89**(11), 465–482 (2019)
50. Toro, E.F.: Riemann Solvers and Numerical Methods for Fluid Dynamics: A Practical Introduction. Springer, Berlin Heidelberg (2009)
51. Toro, E.F., Spruce, M., Speares, W.: Restoration of the contact surface in the hll-riemann solver. *Shock waves* **4**(1), 25–34 (1994)
52. Touma, R., Klingenberg, C.: Well-balanced central finite volume methods for the ripa system. *Applied Numerical Mathematics* **97**, 42–68 (2015)
53. Touma, R., Koley, U., Klingenberg, C.: Well-balanced unstaggered central schemes for the euler equations with gravitation. *SIAM Journal on Scientific Computing* **38**(5), B773–B807 (2016)
54. Turkel, E.: Preconditioned methods for solving the incompressible and low speed compressible equations. *Journal of computational physics* **72**(2), 277–298 (1987)
55. van Leer, B.: Towards the ultimate conservative difference scheme. V – A second-order sequel to godunov’s method. *Journal of Computational Physics* **32**, 101–136 (1979). DOI 10.1016/0021-9991(79)90145-1

- 
56. Varma, D., Chandrashekar, P.: A second-order, discretely well-balanced finite volume scheme for euler equations with gravity. *Computers & Fluids* (2019)
  57. Xing, Y., Shu, C.W.: High order well-balanced weno scheme for the gas dynamics equations under gravitational fields. *Journal of Scientific Computing* **54**(2-3), 645–662 (2013)
  58. Xing, Y., Shu, C.W., Noelle, S.: On the advantage of well-balanced schemes for moving-water equilibria of the shallow water equations. *Journal of scientific computing* **48**(1-3), 339–349 (2011)